Pedro
José da Silva
Gonçalves

Técnicas de Igualização Não Linear para Sistemas de Comunicações Móveis 5G NR

Non-Linear Equalizer Techniques for 5G NR Mobile Communications Systems

Universidade de Aveiro
2021

Pedro José da Silva Gonçalves

Técnicas de Igualização Não Linear para Sistemas de Comunicações Móveis 5G NR

Non-Linear Equalizer Techniques for 5G NR Mobile Communications Systems

Dissertação apresentada à Universidade de Aveiro para cumprimento dos requisitos necessários à obtenção do grau de Mestre em Engenharia Eletrónica e Telecomunicações, realizada sob a orientação científica do Doutor Adão Silva, Professor associado da Universidade de Aveiro, e do Doutor Pedro Pedrosa, Investigador Auxiliar no Instituto de Telecomunicações de Aveiro.

.

This work is supported by the European Regional Development Fund (FEDER), through the Competitiveness and Internationalization Operational Program (COMPETE 2020) of the Portugal 2020 framework, Regional OP Centro (CENTRO 2020), Regional OP Lisboa (LISBOA 14-20) and by FCT/MEC through national funds, under Project MASSIVE5G (AAC no 02/SAICT/2017)

o júri / the jury

presidente / president

Prof. Doutor Pedro Miguel Ribeiro Lavrador
Professor Auxiliar da Universidade de Aveiro

vogais / examiners committee

Prof. Doutor Rui Miguel Henriques Dias Morgado Dinis
Professor Associado com Agregação da Universidade Nova de Lisboa (Arguente)

Prof. Doutor Adão Paulo Soares da Silva
Professor Associado da Universidade de Aveiro (Orientador)

agradecimentos / acknowledgements

A realização desta dissertação não teria sucesso sem a colaboração dos orientadores a quem eu gostaria de agradecer.
Um muito obrigado pela coordenação e pela disponibilidade ao longo deste tempo ao Professor Dr. Adão Silva e ao Dr. Pedro Pedrosa, que muito bem representam os docentes ao nível das instituições do ensino Superior.
Para finalizar gostaria também de agradecer à Universidade de Aveiro, ao Departamento de Eletrónica, Telecomunicações e Informática e ao Instituto de Telecomunicações por garantirem as condições de trabalho e aprendizagem necessárias à realização desta dissertação.

Palavras Chave

5G NR Numerologia, OFDM, Uplink, DFT-s-OFDM, Canais-TDL, Igualizadores lineares na frequência, IB-DFE, BER

Resumo

Devido ao aumento de transmissões com altas taxas de transferência de dados, necessidades de suportar um maior número de utilizadores e constantes pressões feitas pelo mercado das telecomunicações, novas tecnologias têm sido desenvolvidas. Um dos casos destas novas tecnologias é o 5G New Radio (NR), oferecendo taxas de transmissão de dados muito elevadas, melhor eficiência espectral e menor latência quando comparado a tecnologias anteriores. Com o aumento exponencial das comunicações sem fios, surge então problemas relacionados com interfências levando assim à uma diminuição do desempenho geral do sistema. Orthogonal frequency division multiplexing (OFDM) foi durante os últimos anos uma técnica de modelação de dados que serviu como base para transmissões de dados mais eficientes. Contudo, a principal desvantagem do OFDM é o seu elevado *peak-to-average ratio* (PAPR), motivando assim à procura de técnicas de modelação mais promissoras. Portanto, uma das melhorias que o 5G oferece é a possibilidade de usar técnicas de transmissão de blocos no uplink como a *discrete Fourier transform spread orthogonal frequency-division multiplexing*(DFT-s-OFDM). Em comparação com o OFDM, esta técnica de transmissão possui um baixo valor de PAPR, sendo então menos sensível às distorções não-lineares causadas pelo amplificador de potência (AP). Esta técnica de transmissão oferece uma melhoria significativa no desempenho geral dos sistemas, pois consegue lidar com canais que possuem um forte desvanescimento selectivo na frequência ao mesmo tempo que fornece ligações com altas taxas de transmissão. O desempenho do DFT-s-OFDM pode ser melhorado com o recurso a igualizadores não-lineares no domínio da frequência, como o *iterative block decision-feedback equalizer*(IB-DFE). Esta dissertação têm com principal objectivo, a implementação e o estudo de sistemas de igualizadores para sistemas mono e múltiplo utilizador, baseado no modelo IB-DFE, aplicado a DFT-s-OFDM 5G. São considerado dois casos distintos: *single-user* e *multi-user*, como já foi referenciado. Na primeira abordagem, *single-user*, cada utilizador é transmitido em diferentes subportadoras não havendo assim interferência entre os vários utilizadores, tendo o igualizador de lidar com interferência entre símbolos (ISI). No segundo procedimento, *multi-user*, foi considerado um cenário onde os vários utilizadores partilham as mesmas subportadoras, sendo assim transmitidos no mesmo canal físico para a estação base (BS). É assumido que a BS está equipada com múltiplas antenas, e os terminais dos utilizadores com uma antena apenas. Nesta situação como os vários utilizadores partilham os mesmos recursos o nosso equalizador têm que lidar com ambas as interferências, ISI e *multi-user* interferência (MUI). O igualizador não linear vai ser desenvolvido para várias configurações de antenas na estação base, com o intuito de esplorar a diversidade espacial de maneira a aumentar a relação sinal-ruído (SNR) e assim reduzir a taxa de erros de bits (BER). Ambos os cenários vão ser implementados e avaliados segundo as várias numerologias e TDL modelos de canais, definidos pelos relatórios técnicos do 5G NR.

Keywords 5G NR Numerology, OFDM, Uplink, DFT-s-OFDM, TDL-channels, Frequency Equalizers, IB-DFE, BER

Abstract

Due to the increase of data rates, users and the pressure made by the telecommunication market, new technologies have emerged to supply their necessities. 5G New Radio (NR) appears then, offering higher data rates, better spectral efficiency and lower latency when compared to the previous mobile networks technologies. With the increase of devices with wireless connections, interference problems appears causing a reducing in the system performance. In the last years, orthogonal frequency division multiplexing (OFDM) was a modulation technique that provided more efficient transmissions. However, the main disadvantage of this technique, is its higher peak-to-average ratio (PAPR), motivating then the search for more promising modeling techniques. So, one advantage that 5G offers is the possibility of using techniques in the uplink (UL) like the discrete Fourier transform spread orthogonal frequency-division multiplexing (DFT-s-OFDM). Comparing with OFDM, the advantage of this transmission technique is its lower (PAPR), being then less sensitive to non-linear distortions caused by the power amplifier (PA). This type of techniques are important for the overall system performance, as they can handle transmission channels experiencing strong frequency selectivity while still providing transmissions with high data rates. DFT-s-OFDM performance can be improved using non-linear equalizers in the frequency domain. One example of these equalizers is the iterative block decision-feedback equalizer (IB-DFE). In this dissertation we implement and evaluate single and multi-user nonlinear equalizers based on IB-DFE approach for DFT-s-OFDM 5G NR systems. It is considered two main different scenarios:single-user and multi-user cases. In the first one, the data of each each user is transmitted by different set of carriers and therefore there is no multi-user interference and the equalizer only needs to deal with inter-symbol interference (ISI). In the second case, the same set of carries are allocated to the several users, with the base station equipped with multiple antennas and the user terminal with a single antenna. Therefore the equalizer must deals with both inter-symbol-interference and multi-user interference (MUI). The nonlinear equalizers are designed for different number of antennas at the receiver terminal in order to exploit the space diversity and increase the Signal-to-Noise Ratio (SNR) and consequently reduce the Bit Error Rate (BER). The implemented single/multi-user equalizers are evaluated under several TDL channel models and for different numerologies defined in the 5G NR.

Contents

List of Figures

List of Tables

Glossary

1G First Generation
2G Second Generation
3G Third Generation
3GPP Third Generation Partnership Project 1
3GPP2 Third Generation Partnership Project 2
4G Fourth Generation
5G Fifth Generation
ADC Analog-to-Digital Converter
AMPS Analogue Mobile Phone System
BER bit error rate
BPSK Binary Phase Shift Keying
BWP Bandwidth Part
CDMA Code Division Multiple Access
CP cyclic prefix
CP-OFDM cyclic prefix–OFDM
CRB Common Resource Blocks
DAC Digital-to-Analog Converter
DFEs decision feedback equalizers
DFT-s-OFDM discrete Fourier transform spread orthogonal frequency division multiplexing
DL downlink
DS Delay spread
EGC Equal Gain Combining
eMBB Enhanced Mobile Broadband
EPC Enhanced Packet Core
ETSI European Telecommunications Standards Institute
FDD frequency-division duplex
FDMA Frequency Division Multiple Access
FFT Fast Fourier Transform
FR1 Frequency Range 1
FR2 Frequency Range 2
GSM Global System for Mobile Communication
HSPA High Speed Downlink Packet Access
IB-DFE iterative block-decision feedback equalizer
ICI inter-carrier interference
IFFT Inverse Fast Fourier Transform
IMT International Mobile Telecommunications
IMTS Improved Mobile Telephone Service

IoT	Internet of Things
IP	Internet Protocol
ISI	inter-symbol interference
ITU	International Telecommunications Union
LOS	Line-of-Sight
LTE	Long Term Evolution
MFB	matched-filter bound
MIMO	Multiple-Input Multiple-Output
MMSEC	Minimum Mean Square Error Combining
mMTC	Massive Machine- Type Communication
MRC	Maximum Ration Combining
MSE	Mean Squared Error
NLOS	Non-Line-of-Sight
NR	New Radio
NTT	Nordic Mobile Telephone
OFDM	orthogonal frequency division multiplexing
OFDMA	orthogonal frequency division multiple access
PA	power amplifier
PAPR	peak-to-average power ratio
PRB	Physical Resource Blocks
QAM	Quadrature Amplitude Modulation
QoS	Quality of Service
QPSK	Quadrature Phase Shift Keying
TACS	Total Access Communication System
TDD	time-division duplex
TDL	Tapped-Delay-Line
TDMA	Time Division Multiple Access
RB	Resource Blocks
RMS	root mean square
SC-FDMA	single carrier frequency division multiple access
SIMO	Single-Input Multiple-Output
SINR	Signal to Interference plus Noise Ratio
SISO	Single-Input Single-Output
SNR	signal-to-noise ratio
SQNR	Signal-to-Quantization Noise Ratio
UE	user equipment
UL	uplink
URLLC	Ultra-Reliable and Low Latency Communications
V2X	Vehicle-to-Everything
VRB	Virtual Resource Blocks
WCDMA	Wideband Code Division Access
ZFC	Zero Force Combining

CHAPTER 1

Introduction

This chapter presents the background and evolution of the communications systems history, then the motivations and objectives that serve as basis to the this dissertation and finally, an outline of the document is presented.

1.1 The Road to the 5th Generation (5G)

Mobile communications data usage has experienced an enormous growth over the last 40 years expected to continue growing even more in the future. 5G celular radio communications represents a big advance in mobile network capabilities and will take the traditional mobile broadband to the extreme in terms of data rates, capacity, and availability. In addition, 5G will enable new services including industrial Internet of Things (IoT) connectivity and critical communication, expected to impact all sectors of society by providing increased efficiency and productivity.5G targets were set very high with data rates up to 20Gbps and capacity increases of up to 1000 times, with flexible platforms for device connectivity, ultra-low latency, and high reliability(Figure 1.1) [1].

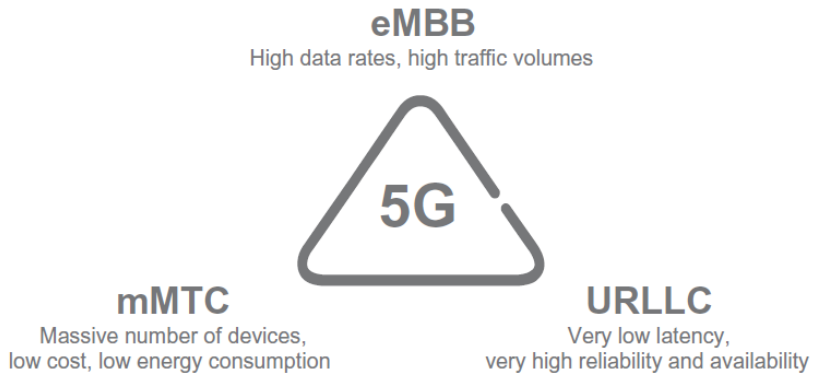

Figure 1.1: 5G use-case classification [1].

Today, mobile communications services are used by a significant percentage of the world's population. According to Ericsson Mobility Report, despite the uncertainty caused by COVID-19, service providers continue to switch on 5G and the estimate is that by the end of 2021 there will be approximately 580 million 5G subscriptions[2]. To know how mobile communications systems evolved important since it allows us to better understand how modern mobile communications systems are now able to deliver such remarkable services at scale (Figure 1.2).

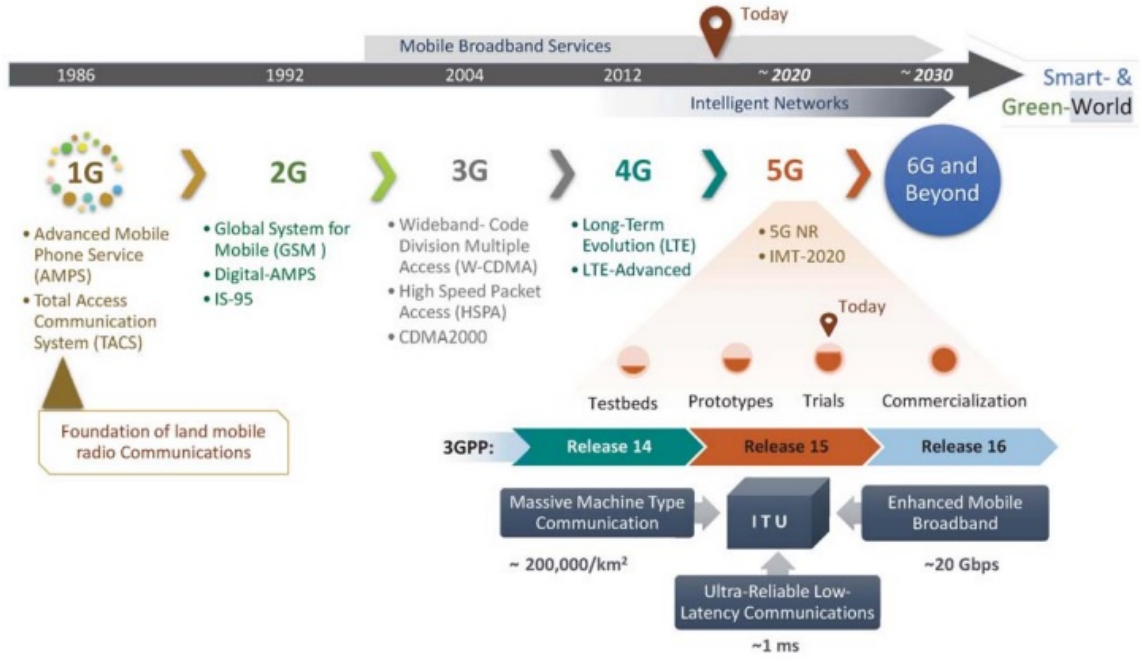

Figure 1.2: Standards evolution mobile communications systems [3].

A new generation of mobile communications standards has appeared about every tenth year, the first commercial cellular telephone system in the United States, known as Analogue Mobile Phone System (AMPS), was placed into operation in late 1983 and the bandwidth for the channel were 30kHz [4]. Each country developed their own First Generation (1G) standards , the Nordic Mobile Telephone (NTT) used in eastern Europe and Russia , AMPS North America, Total Access Communication System (TACS) in the United Kingdom, and (TZ-801/2/3) in Japan. The first-generation systems were analog voice-only mobile-telephony systems, available on a national basis, without international roaming, or a very limited one, and targeting a very selected group of people. The first generation uses analog modulation and frequency division multiple access (FDMA) as the main techniques (Figure 1.3).

By slicing the frequency channel into several uncorrelated sub-channels and by allocating the different sub-channels to different users, multiple users can be allocated in the same time-slot. A protective frequency band usually needs to be configured between sub-channels to resist non-ideal filter impairments, adjacent channel interference, and frequency spread caused by Doppler shift [5]. Due to the drawbacks of FDMA based analog cellular systems, such as low spectral efficiency, security risks and weak interference resistance ability, it was

abandoned as a result of the market competition.

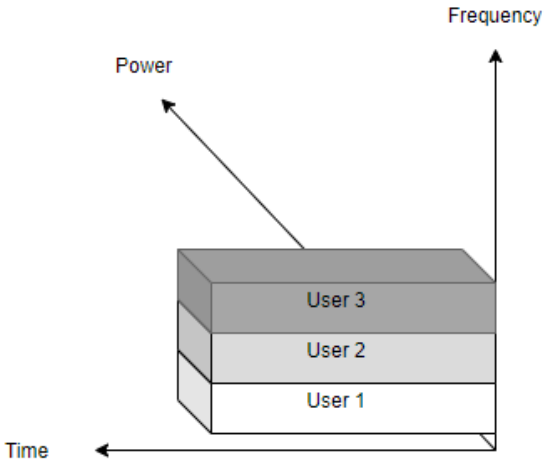

Figure 1.3: FDMA technique.

Due to the several limitations of the 1G, Improved Mobile Telephone Service (IMTS) appears and 2nd generation are created , the IMTS-MJ system that uses 11 channels with 150 MHz carrier frequencies, and the IMTS-MK system that uses 12 channels with 450 MHz carrier frequencies [6].

The Second Generation (2G) of mobile communication appeared in the early 1990s. The principal change from 1G was to use digital communication instead of the analog ones .The first standard was the Global System for Mobile Communication (GSM) and was launched in 1991. Initially different countries developed their own second-generation technologies, GSM by several European countries, D-AMPS (Digital AMPS), developed in Japan and North American, IS-95 and IS-136, based on code division multiple access (CDMA) and time division multiple access (TDMA) technique, respectively [7].

Over the course of the years the support for packet data services has been extended, these extensions are referred as 2.5G. EDGE is a well known example of a 2.5G technology [8]. The GSM-based 2G standards adopted TDMA, (Figure 1.4), and narrowband CDMA. With TDMA the data to be transmitted is divided into different slots, each user occupies one respective slot. However, the different users cannot transmit simultaneously, they transmit in orthogonal slots. CDMA is a technique which transmits the data based on a unique code sequence assigned for each channel.

The main problem of TDMA-based transmissions is the synchronization needed between the different users. In the downlink, and for flat channels, the users transmit in orthogonal time-slots, and the signal at the receiver maintains its orthogonality, but for the uplink, the transmission from the different users is sent in different channels each with a different delay , so synchronization is necessary to ensure that the received signals are orthogonal in time. As a result,a guard band is needed between channels to prevent the detrimental impact of multi-path, and synchronization errors [9].

The Third Generation (3G) of mobile communications was introduced in the 2000. The

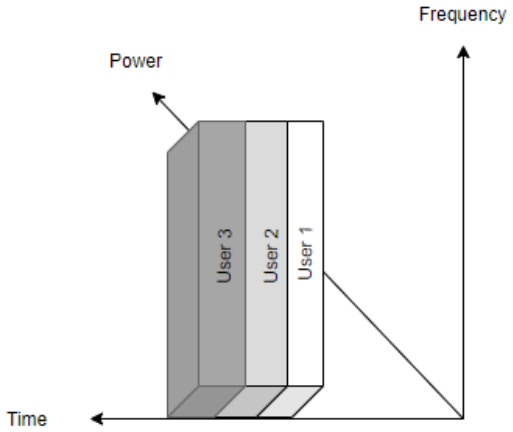

Figure 1.4: TDMA technique.

Table 1.1: 2G mobile communications standards [6].

	GSM	IS-95	PDC	IS-139
Uplink frequencies(MHz)	890-915	824-849	940-956 1409-1453	824-849
Downlink frequencies (MHz)	935-960	869-894	810-826 1477-1501	869-894
Bandwith (kHz)	200	25	1250	30
Number of users	8	64	3	3
Number of channels	1000	2500	1600	832
Modulation	GMSK	BPSK/ QPSK	$\pi/4-D-$ QPSK	$\pi/4-D-$ QPSK
ISI reduction	Equalizer	RAKE, SHO	Equalizer	Equalizer
Multiple-acess	TDMA	CDMA	TDMA	TDMA

principal innovation in 3G was the use of packet-based data communication, enabling fast wireless internet access, starting a new era of mobile internet. Then maximum date rate of 3G was around 2Mbps, which is approximately four times faster than 2G. 3G was designed to respect the IMT-2000 standard, created by the International Telecommunications Union (ITU)[10]. The main transmission schemes of 3G include, Wideband Code Division Access (WCDMA), CDMA-2000 and TD-SCDMA, witch CDMA, (Figure 1.5), is the base technique for 3G. WCDMA and CDMA-2000 are evolutions of GSM and IS-95 CDMA, respectively, while TD-SCDMA is a new standard proposed for the operation in unpaired spectrum using time-division duplexing. Due to popularity, GSM it is still up to date the most widespread mobile communications in the world.

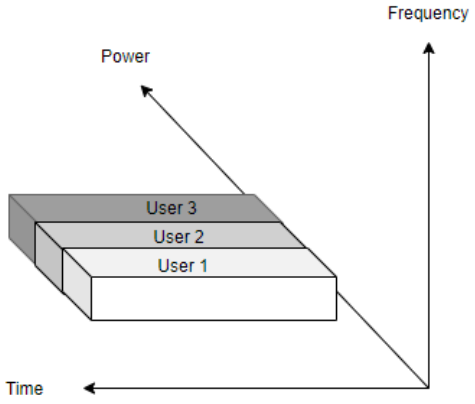

Figure 1.5: CDMA technique.

The CDMA 2000 system was the commercially successful 3G standard in North America and South Korea, standardized by Third Generation Partnership Project 2 (3GPP2). In this technique different users choose different spreading codes and occupy the same spectral resources simultaneously [11]. There are differences between uplink (UL) (forward channel) and downlink (DL) (reverse channel). In downlink, CDMA applies orthogonal spreading code, and in the UL, we have non-orthogonal spreading code. By using this non-orthogonal spreading code we can have an increased number of users on UL but then inter-user interference is introduced [12].

The Fourth Generation (4G), represented by the LTE technology, was designed to support faster data rates, lower latency and higher capacity than 3G, starting a new era of real-time streaming. The LTE standard was released in 2009 as (3GPP) release 8 [13].

The main technology improving the data rates were a new multiple access technique referred to as orthogonal frequency division multiple access (OFDMA), (Figure 1.6), and MIMO communications.

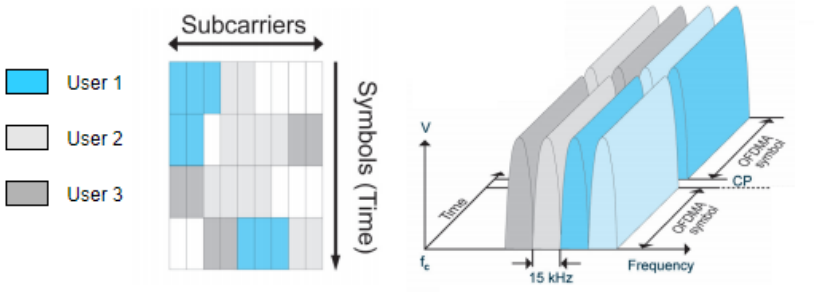

Figure 1.6: OFDMA technique [14].

OFDMA is a multiple access method based on the technique of orthogonal frequency division multiplexing (OFDM). OFDM is similar to FDMA but much more spectrally efficient since the sub-channels are spaced much closer. This is done by finding frequencies that are orthogonal, thus allowing the spectrum of each subcarrier to overlap those of other sub-carriers without interference. Because of this, we are able to achieve multi-user access by allocating different subcarrier to a single user in different slots and distinguishing users through the subcarrier frequencies [15]. In order to continue to ensure a great spectral efficiency and, at the same time, lower peak-to-average power ratio (PAPR), a new hybrid modulation scheme dubbed single carrier frequency division multiple access (SC-FDMA) was developed [16].

Other radical aspect of 4G is the flat radio and core network architecture, which means fewer nodes and a less hierarchical structure for the network. Known as Enhanced Packet Core (EPC), it replaces the architecture used by GSM and WCDMA/High Speed Downlink Packet Access (HSPA).

LTE operates in both paired and unpaired spectrum frequency bands. This requires flexibility in the duplex arrangement. For this reason, LTE supports both frequency-division duplex (FDD) and time-division duplex (TDD) operations. The FDD and TDD bandwidths are defined by Third Generation Partnership Project 1 (3GPP) and depend on the users geographical location. 3GPP Release 13 specifications for LTE includes 32 frequency bands for FDD and 12 for TDD [17].

The last phase of the LTE technology was defined in Releases 13–15 under the name LTE-Advanced Pro. Release 13 was completed in June 2016, Release 14 in June 2017, and Release 15 in September 2018. The 3GPP Release 15 marks the first release for 5G New Radio (NR). On a high level, the 5G NR air interface looks very similar to LTE since it was designed initially for one specific use case only, high-speed Internet access. Because of the market pressure, it was decided to launch the first 5G system specifications as quickly as possible .

As mentioned, this increasing demand for high throughput connections, to decrease latency, to have better quality of service, the need to serve a greater number of mobile users per cell, to increase the volume of data over wireless networks, with more cost efficient, are among the reasons that have led to the appearance of the 5G NR. Besides increasing the operating bandwidth, one of the main enhancements brought by this next generation is the improvement of spectral efficiency usage when compared with previous generations. New features and use cases will be introduced continuously throughout the development of this technology, bringing much more than just performance enhancements. One of this improvements is the use of 5G technologies in the IoT and vertical industries, that will provide new business opportunities for network operators. Therefore 5G will have to be widely deployed and adapted in order to comply with the diversity of service requirements. IMT has defined three main uses cases for 2020 and beyond [18]: Enhanced Mobile Broadband (eMBB), Massive Machine- Type Communication (mMTC) and Ultra-Reliable and Low Latency Communications (URLLC). More details about this uses cases will be provided in on Chapter 2.

1.2 Motivation and Objectives

The 5^{th} Genaration radio access technology is expected to take a huge leap forward compared to previous generations by enabling even better wireless connectivity for essentially every kind of device or application that may benefit from being connected. Technologies like automated intelligence, autonomous vehicles, the IoT, high quality Internet Protocol (IP) telephony, broadcasting televisions (TVs) and high-speed data communication, among others, demands higher spectrum efficiency, larger capacity, more connectivity, and lower latency.

To satisfy the 5G network requirements, multi-carrier modulation techniques need to be more flexible and efficient. OFDM is used in systems partially because it allows simple receiver architectures and permits flexible access to frequency-domain resources to achieve high spectral efficiency. On one hand, since OFDM signals have high PAPR, the UL of 5G systems will also adapt the discrete Fourier transform spread orthogonal frequency division multiplexing (DFT-s-OFDM) waveform to reduce the user equipment (UE) power consumption and power amplifier (PA) cost. In 5G NR, the modulation used for DL and for high data-rate UL scenarios, is the cyclic prefix–OFDM (CP-OFDM). On the other hand, in scenarios where we have limited power, the modulation used is DFT-s-OFDM, as mentioned before. In fact, it is very important to deal with PAPR reduction in OFDM systems to avoid signal degradation [19]. In order to address this issue DFT-s-OFDM, a modified form of OFDM with similar performance, but presenting low PAPR and allowing simple frequency-domain linear equalization was introduced for the UL of 5G NR. It is known that linear equalizers are not the best for DFT-s-OFDM or SC-FDMA, since these are not capable of dealing with the residual interference. In fact that nonlinear/iterative equalizers, particularly those based on the iterative block-decision feedback equalizer (IB-DFE) principle, outperforms the linear ones and have excellent performance-complexity tradeoffs [20].

The IB-DFE based on feedforward and feedback filters implemented in the frequency-domain and is capable of minimizing the impact of the channel noise, and inter-symbol interference (ISI) of time-dispersive channels [21]. Moreover, it has been proved capable of performing close to the matched-filter bound (MFB) in rich multipath channels, especially when combined with diversity techniques [22]. Finally, its low-complexity design and power efficiency, are important for mobile terminals for efficient battery preservation and the usage of low-cost amplifiers.

The scope of this work is the implementation and evaluation of single and multi-user nonlinear equalizers based on the IB-DFE approach for DFT-s-OFDM modulations, considered in the UL of 5G NR. We will consider two main different scenarios, the *single user* case in the sense that each user is assigned a different set of carriers and therefore there is no multi-user interference and the equalizer only needs to deal with ISI, and the *multi-user* case where the same set of carriers is assigned to different users, and therefore the equalizer must deals with both ISI and multi-user interference. The latter scenario is more complex but allows to boost the data rate, which is fundamental to meet the throughput requirements of future applications. Additionally, the equalizers are designed considering a multiple number of antennas at the

receiver, in order to exploit space diversity and, thus increase the signal-to-noise ratio (SNR). Consequently, the bit error rate (BER) will be reduced. Finally, the performance of the single/multi-user equalizers is evaluated under several channel models and for the different numerologies defined in the 3GPP 5G NR technical reports.

1.3 Dissertation outline

After this introductory chapter in which the history and evolution of mobile radio communications standards were briefly discussed, and the motivation and objectives of this dissertation presented, in Chapter 2 an overview of the 5G NR is presented. We start by introducing the challenges and keys specifications of 5G communication systems and then discuss performance requirements and spectral allocation. Additionally, a discussion on the characteristics of the channels models profiles considered in this dissertation is also included.

In chapter 3 we discuss the basic principles of OFDM like modulation, orthogonality and the introduction of a (CP) to avoid interference. We focus on explaining the most critical physical layer concepts of 5G NR.

Next, in Chapter 4, the DFT-s-OFDM modulation scheme, adopted in the UL of 5G NR, is studied. Particularly the transmitter and receiver blocks are discussed. Then the single-user equalizers usually employed in both SISO and SIMO systems are presented. Finally, we conclude Chapter 4 presenting and discussing the performance of these equalizers for several 5G scenarios.

In Chapter 5 we present the IB-DFE for DFT-s-OFDM. Chapter 5 is divided into two parts. In the first part a single-user IB-DFE is proposed and a mathematical analysis of its performance conducted, followed by presentation and discussion of simulation results. In a second part of Chapter 5, a multi-user IB-DFE is discussed. The proposed single/multi-user equalizers have their performance evaluated for multiple channel models and different 5G NR numerologies, as defined in Chapter 2 and 3.

Finnaly, Chapter 6, concludes this dissertation with the discussion of its main results and future work.

CHAPTER 2

5G New Radio Overview

5G represents a major step in mobile network capabilities. Firstly, this chapter provides an introduction about the 5G NR. Following, 5G use cases with each specific requirements and range of operating frequencies are presented. Finally, the 5G channels models defined by European Telecommunications Standards Institute (ETSI) reports are presented in the last section.

2.1 Introduction

The need for great increases in data capacity, speeds and low latencies make way for the next generation, Fifth Generation 5G NR. Discussions about 5G started around 2012, the term 5G is used to refer to specific new 5G radio access technology. At the end of 2018, 5G NR, the next generation cellular standard defined by 3GPP is released in Release 15 [23].

The commercialization of 5G started by the end of 2020 in some countries. 5G will continue on the path of LTE, enabling even higher data rates and even higher efficiency for mobile broadband. 5G technology will provide the necessary infrastructure and resources to several vertical industries so that they can also provide new services to users. Fifth-generation, it's not just a specific radio-access technology but a service that will enable a wide range of new services envisioned by future mobile communication. Health-care and automotive industry, are some examples of industry sectors that 5G is expected to revolutionize. On automotive industry we have the self-driving cars that requires latency close to few milliseconds, for example.

Table 2.1: Comparison of performance between 5G-NR and LTE [24].

Feature	LTE	NR
Peak data rate	1 Gbps	20 Gbps
Use experienced data rate	10 Mbps	100 Mbps
Spectrum effiency	1x	3x
Mobility	350 km/h	500 km/h
Latency	10 ms	1 ms
Connection density	$10^5 devices/km^2$	$10^6 devices/km^2$
Network energy effiency	1x	100x
Area traffic capacity	0.1 Mbps/m^2	10 Mbps/m^2

5G aims to support much higher systems capacity than the current 4G (see Table 2.1). Fifth Generation of Mobile Communications (5G) will differentiate itself by showcasing new improvements such as:

- 10x throughput velocities;
- 10x lower latencies;
- 10x density connections;
- 3x spectrum efficiency;

2.2 The 5G uses cases

As we have seen previously on Chapter 1, 5G with these more advanced capabilities, can support diverse usage scenarios and applications. ITU has defined three distinct classes of uses cases 5G under IMT 2020 and beyond [18]. The three scenarios defined were, (Figure 2.1) :

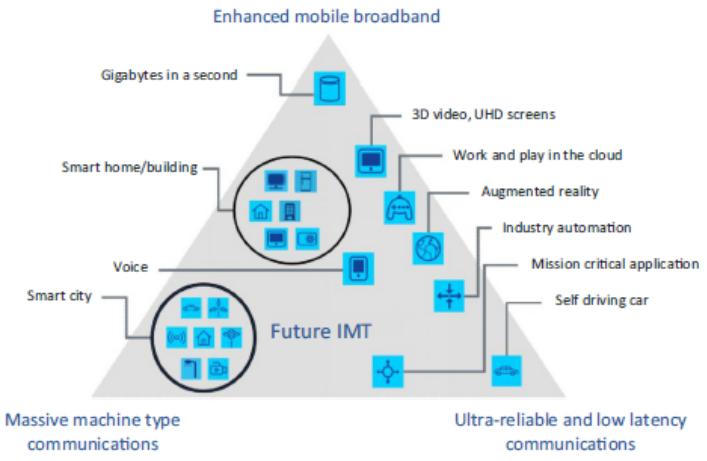

Figure 2.1: 5G IMT-2020 use cases and mapping to usage scenarios [18].

- **eMBB**

  eMBB can be considered as a straightforward extension of the mobile broadband services of today. It is characterized by high data rates and large traffic volumes.

Example eMBB services are the proliferation of smart wireless devices along with multimedia content such as high definition (HD) video, online gaming, AR, virtual reality (VR) and 4k streaming. 5G will deliver improved user experience by supporting ultra-broadband services for eMBB applications. So, the main objective is to provide better indoor and outdoor broadband services to users by offering better data rate, spectral efficiency, capacity, coverage, latency and user density [25].

- **mMTC**

  mMTC mainly refers to the IoT services that are characterized by a massive number of devices, where are interconnected to realize a fully connected society. These devices typically requires low complexity, long battery life time and significant coverage extension. mMTC use can be realized as IoT, asset tracking, smart cities, smart homes, energy monitoring and remote monitoring. Such services usually have relaxed latency requirements, and each device typically does not require support of high data rates [25].

- **URLLC**

  URLLC is a service category providing data delivery with precise reliability, very-low latency and availability. Besides mMTC, URLLC is another key component for building the IoT platform for modern applications. Some of examples of URLLC use case are Vehicle-to-Everything (V2X), remote medical procedures, industrial automation and smart grids [25].

2.3 Technical Performance Requirements

As seen from the uses cases, the fifth generation system will be maneuvering diverse use cases with specific requirements for each case. The minimum technical performance requirements for 5G were approved by [18]. The Table 2.2 is a visualization that summarizes the number of key parameters along with the use case for which they are relevant, for 5G.

- **Peak data rate:** Is the maximum achievable data rate under ideal conditions (in bit/s). Is the received data bits assuming error-free conditions assignable to a single mobile station, when all assignable radio resources for the corresponding link direction are utilized (i.e., excluding radio resources that are used for physical layer synchronization, reference signals or pilots, guard bands and guard times) [26]. The peak data rate depends on the peak spectral efficiency, which is the peak data rate normalized by the bandwidth [7]:

  Peak data rate = System bandwidth x Peak spectral efficiency

- **User experienced data rate:** Is the data rate that can be achieved across a large coverage area to a mobile user/device (in Mbit/s or Gbit/s).
- **Latency:** It is defined as the time needed from when the source sends a data packet until it reaches your destination (in ms).
- **Mobility:** Is the maximum mobile station speed at which a defined Quality of Service (QoS) can be achieved, it is expected to reach values up to 500 km/h [18];

Table 2.2: Minimum technical requirements of 5G [26].

Technical requirement	Use scenario applicability	Target Balue
Peak Data Rate	eMBB	DL: 20 Gbps UL: 10 Gbps
Peak Spectral Efficiency	eMBB	DL: 30 bps/Hz UL: 15 bps/Hz
User Experienced Data Rate	eMBB	DL: 100Mbps UL: 50 Mbps (Dense Urban)
5% User Spectral Efficiency	eMBB	DL: 0.3 bps/Hz UL: 0.21 bps/Hz (Indoor Hotspot)
		DL: 0.225 bps/Hz UL: 0.15 bps/Hz (Dense Urban)
		DL: 0.12 bps/Hz UL: 0.045 bps/Hz (Rural)
Average Spectral Efficiency	eMBB	DL: 9 bps/Hz/TRxP UL: 0.21 bps/Hz/TRxP (Indoor Hotspot)
		DL: 0.225 bps/Hz/TRxP UL: 0.15 bps /Hz/TRxP (Dense Urban)
		DL: 12 bps/Hz/TRxP UL: 0.045 bps/Hz/TRxP (Rural)
Area Traffic Capacity	eMBB	DL: 10 Mbps/m^2($IndoorHotspot$)
User Plane Latency	eMBB, URLLC	4 ms for eMBB 1 ms for URLLC
Control Plane Latency	eMBB, URLLC	20 ms for eMBB and URLLC
Connection Density	mMTC	1,000,000 devices/Km^2
Energy Efficiency	eMBB	Support high sleep ratio and long sleep duration
Mobility	eMBB	Up to 500 Km/h
Mobility Interruption Time	eMBB, URLLC	0 ms
Bandwith	eMBB	At least 100 MHz, up to 1Ghz for higher frequency bands

- **Spectrum efficiency:** Average data throughput per unit of spectrum resource and per $cell^3$ (bit/s/Hz). The target for IMT-2020 was set to three times the spectrum efficiency target of 4G, but the levels achieved with 4G systems are already very high [7].
- **Network energy efficiency:** Is the capability of information bits that can be transmitted/received, per unit of energy consumption (in bit/Joule). Another important aspect is the low energy consumption when there is no data.
- **Area traffic capacity:** Is the total traffic throughput served per geographic area (in Mbit/s/m^2). The throughput is the number of correctly received bits.
- **Connection density:** Is the total number of connected and/or accessible devices per km^2.

2.4 **5G Spectrum**

5G NR was designed to operate in a wide range of frequencies. Every generation emergence of mobile communication has expanded the range of spectrum in with the wireless-access technology can operate. The first-generation systems were limited to operation below 1GHz, the second-generation below 1 GHz initially but later expanded into the 1.8/1.9 GHz bands and the 3G was the first mobile communication system above 2 GHZ, more specifically into the so-called IMT core bands around 2.1 GHz. Unlike LTE, where support for licensed spectrum at 3.5 GHz and unlicensed spectrum at 5GHz, 3GPP has decided that NR will already from the start support operations, from below 1 GHz up to 90 GHz, for operation in both licensed, shared and unlicensed spectrum.

It should be noted that the expansion to higher-frequency bands does, in no way, imply that the later generations cannot be deployed in lower-frequency bands, the expansion to higher-frequency bands is mainly driven by a need for more spectrum providing higher system capacity to handle the continuously increasing traffic volumes, like the demanding eMBB usage scenarios and related new services.

New bands are defined continuously by 3GP, for the new NR specifications. In 5G-NR specifications, paired bands are used for FDD operation, while unpaired bands are used for TDD operation. On paired bands, separated frequency ranges are assigned for uplink and downlink, on unpaired bands, a single shared frequency range are assigned for uplink and downlink.Some ranges are also defined for Supplementary Downlink (SDL) or Supplementary Uplink (SUL) bands.

In 5G-NR there will be two ranges for frequency bands, according to [23]:

- FR1- From 450 MHZ to 6GHz (see Table 2.3)
  - The range n65 to n256 is reserved for NR bands in frequency range 1
  - Commonly referred to as Sub-6GHz
- FR2- From 24.25 GHz up to 52.6GHz (see Table 2.4)
  - The range n257 to n512 is reserved for new NR bands in frequency range 2
  - Commonly referred to as mmWave (although technically speaking mmWave starts from 30 GHz)

For NR, the letter “n” is preceding the band number to distinguish it from possible LTE deployed in the same band. For example, band n71 is a paired band in the 600MHz frequency for FDD with UL frequency range of 663–698MHz and DL frequency range of 617–652 MHz; band n261 is an unpaired band in the 28 GHz frequency for TDD with UL and DL frequency ranges of 27.50–28.35 GHz. If an LTE band is referred as an NR band, they share the same band number.

Table 2.3: New Radio Frequency Bands in FR1 [1].

NR Band	Uplink Range (MHz)	Downlink Range (MHz)	Duplex Mode	Main Region(s)
n1	1920-1980	2110-2170	FDD	Europe,Asia
n2	1850-1910	1930-1990	FDD	Americas (Asia)
n3	1710-1785	1805-1880	FDD	Europe,Asia (Américas)
n5	824-849	869-894	FDD	Américas,Asia
n7	2500-2570	2620-2690	FDD	Europe,Asia
n8	880-915	925-960	FDD	Europe,Asia
n20	832-862	791-821	FDD	Europe
n28	703-748	758-803	FDD	Asia/Pacific
n38	2570-2620	2570-2620	TDD	Europe
n41	2496-2690	2496-2690	TDD	Us, China
n50	1432-1517	1432-1517	TDD	
n51	1427-1432	1427-1432	TDD	
n66	1710-1780	2110-2200	FDD	Americas
n70	1695-1710	1995-2020	FDD	
n71	663-698	617-652	FDD	Americas
n74	1427-1470	1475-1518	FDD	Japan
n75	N/A	1432-1517	SDL	Europe
n76	N/A	1427-1432	SDL	Europe
n77	3300-4200	3300-4200	TDD	Europe, Asia
n78	3300-3800	3300-3800	TDD	Europe, Asia
n79	4400-5500	4400-5500	TDD	Asia
n80	1710-1785	N/A	SUL	
n81	880-915	N/A	SUL	
n82	832-862	N/A	SUL	
n83	703-748	N/A	SUL	
n84	1920-1980	N/A	SUL	

Table 2.4: New Radio Frequency Bands in FR2 [1].

NR Band	Uplink and Downlink Range (MHz)	Duplex Mode	Main Region(s)
n257	26500-29500	TDD	Asia, Americas (global)
n258	24250-27500	TDD	Europe, Asia (global)
n259	39500-43500	TDD	Global
n260	37000-40000	TDD	Americas (global)
n261	27500-28350	TDD	Americas

2.5 TDL Channels

The channel models selected are preliminary models discussed by ETSI [23] and differentiate between Line-of-Sight (LOS) and Non-Line-of-Sight (NLOS). Frequency-selective channels have become a standard for digital communications. There are 5 different profiles for TDL channels:

- TDL A, TDL B and TDL C corresponds to a NLOS scenario.
- TDL D and TDL E corresponds to a LOS scenario.

One way to represent the impulse response of a multipath channel of the TDL model with N_{taps} number of taps is by the followed form [27]:

$$H(t,\tau) = \sum_{i=1}^{N_{taps}} a_i(\tau)\delta(\tau - \tau_i) \tag{2.1}$$

Here, N_{taps} is the number of active taps, a_i and τ_i are the gain and delay of the ith tap. The total channel model can now be fully characterized by specifying only the desired delay and Doppler spread. The Doppler spectrum for each tap is characterized by a classical (Jakes) spectrum shape and a maximum Doppler shift f_D where [23]:

$$f_D = \frac{|\bar{v}|}{\lambda_0} \tag{2.2}$$

$\bar{v}$ is the vector that represents the velocity, and λ_0 is the wavelength of the carrier frequency. For the taps that follows a Ricean fading distribution the Doppler spectrum contains a peak at the Doppler shift $f_s = 0.7 f_D$ with an amplitude such that the resulting fading distribution has the specified K-factor [23].

TDL model can be scaled in delay so that the model achieves a desired root mean square (RMS) delay spread. The RMS delay spread values for TDL models, on [23], are normalized and can be scaled by the following equation:

$$\tau_{n,scaled} = \tau_{n,model} \times DS_{desired} \tag{2.3}$$

- $DS_{desired}$ is the desired delay spread wanted (in [ns]);
- $\tau_{n,model}$ is the normalized delay presented on the TDL models tables at [23]
- $\tau_{n,scaled}$ represents the new delay value for the n^{th} tap (in [ns]).

On the 2021 technical report from ETSI [28], the delay profiles are simplified from the [23]. The simplifications steps are explained step by step in [28]. Different models are used for FR1 and FR2, in this dissertation, only FR1 TDL channels are covered (TDL A,B and C). The corresponding deployment scenarios are specified in table 2.5 and the tapped delay line models characteristics are specified in tables 2.6, 2.7 and 2.8 .

Table 2.5: Model parameters used for TDL channels [28].

Model	Nº of taps	DS	Maximum excess tap delay	Delay resolution
TDL A	12	30 ns	290 ns	5 ns
TDL B	12	100 ns	480 ns	5 ns
TDL C	12	300 ns	2595 ns	5 ns

Table 2.6: TDL A characterization (DS= 30 ns) [28].

Tap #	Delay (ns)	Power (dB)	
1	0	-15,5	Rayleigh
2	10	0	Rayleigh
3	15	-5.1	Rayleigh
4	20	-5.1	Rayleigh
5	25	-9.6	Rayleigh
6	50	-8.2	Rayleigh
7	65	-13.1	Rayleigh
8	75	-11.5	Rayleigh
9	105	-11.0	Rayleigh
10	135	-16.2	Rayleigh
11	150	-16.6	Rayleigh
12	290	-26.2	Rayleigh

Table 2.7: TDL B characterization (DS= 100 ns) [28].

Tap #	Delay (ns)	Power (dB)	
1	0	0	Rayleigh
2	10	-2.2	Rayleigh
3	20	-0.6	Rayleigh
4	30	-0.6	Rayleigh
5	35	-0.3	Rayleigh
6	45	-1.2	Rayleigh
7	55	-5.9	Rayleigh
8	120	-2.2	Rayleigh
9	170	-0.8	Rayleigh
10	245	-6.3	Rayleigh
11	330	-7.5	Rayleigh
12	480	-7.1	Rayleigh

Table 2.8: TDL C characterization (DS= 300 ns) [28].

Tap #	**Delay (ns)**	**Power (dB)**	
1	0	-6.9	Rayleigh
2	65	0	Rayleigh
3	70	-7.7	Rayleigh
4	190	-2.5	Rayleigh
5	195	-2.4	Rayleigh
6	200	-9.9	Rayleigh
7	240	-8.0	Rayleigh
8	325	-6.6	Rayleigh
9	520	-7.1	Rayleigh
10	1045	-13.0	Rayleigh
11	1510	-14.2	Rayleigh
12	2595	-16.0	Rayleigh

CHAPTER 3

NR Physical Layer concepts

This chapter describes aspects about the physical layer that supports 5G NR, such as waveforms, modulation supported, signals, a more flexible frame structure because of the different numerology and the channel bandwidth. Also introduces the principal characteristics of the frame structures for each numerology.

3.1 Waveform and Orthogonality

OFDM was selected in LTE/LTE-A and continues to be supported in the 5G NR. Uses as a waveform in both uplink and the downlink transmission directions. OFDM is based on multiple subcarries which are partially overlapping each other, but only one has peak amplitude value at a time (Fig 3.1). Overlap of spectral energy does not interfere with the system's ability to recover the original signal. This is achieved by selecting subcarriers that has different frequency domains. The use of orthogonal subcarriers allows more subcarriers per bandwidth resulting in an increase in spectral efficiency.

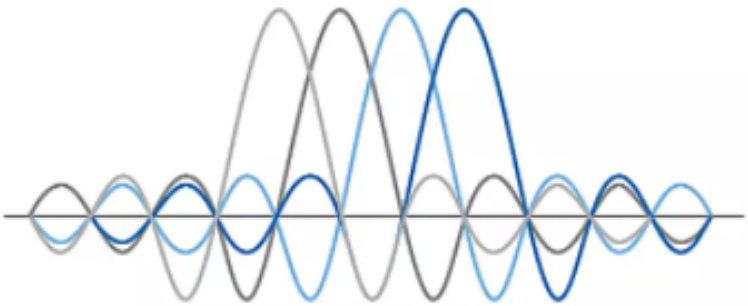

Figure 3.1: OFDM Waveform with 4 subcarriers [29]

Sum up, orthogonality is a property that allows the signals to be perfectly transmitted over a common channel and detected without interference. Set of functions are orthogonal to each other if they match the conditions in the following expression,

$$\int_A^T S_i(t) \times S_j(t)dt = \begin{cases} A & i = j \\ 0 & i \neq j \end{cases} \tag{3.1}$$

It means that if any two different functions within a set are multiplied and integrated over a symbol period, the result is zero for orthogonal functions [30].

3.2 Data Modulation

The downlink and uplink have different modulation schemes, given by specifications on [23]:

- Downlink: Quadrature Phase Shift Keying (QPSK) 16-Quadrature Amplitude Modulation (16QAM), 64-Quadrature Amplitude Modulation (QAM), 256-QAM
- Uplink: QPSK 16QAM 64QAM 256QAM for OFDM with a cyclic prefix (CP) and $\frac{\pi}{2}$-Binary Phase Shift Keying (BPSK), QPSK, 16QAM, 64QAM, 256QAM, for DFT-s-OFDM with a CP.

In LTE, DFT-s-OFDM was already used in the DL, to reduce the PAPR in the UL the SC-FDMA is used. In 5G NR, the uplink have the ability to support both CP-OFDM and DFT-s-OFDM.

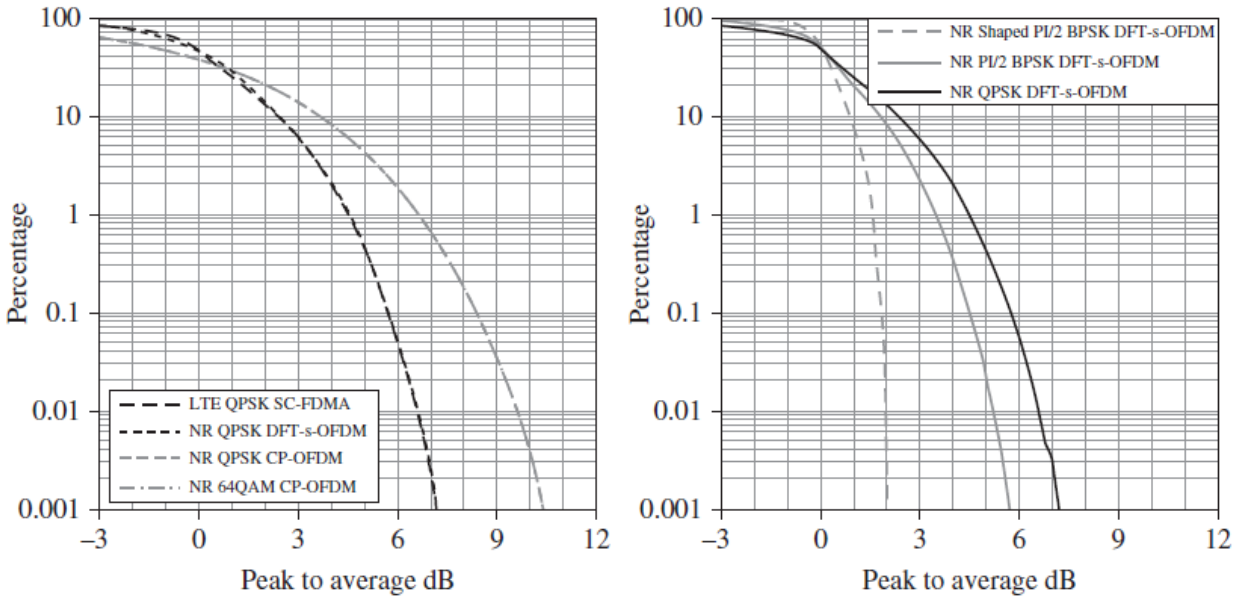

Figure 3.2: Compared PAPR between LTE and 5G NR with different modulations [31]

Analysing the Fig 3.2, we can see that QPSK-modulated DFT-s-OFDM offers a low PAPR, but have limitations such the PAPR increases with higher order modulations, and Resource Blocks (RB) allocations must follow the rule of the equation $N_{RB} = 2^x * 3^y * 5^z$. QPSK CP-OFDM comparing with DFT-s-OFDM has approximately 2.5 dB higher PAPR but don't have the limitations in RB allocations. We can conclude too for higher order modulations the

CP-OFDM is more efficient than DFT-s-OFDM. In this work the modulation covered will be QPSK DFT-s-OFDM.

3.3 Single-Carrier versus Multicarrier Modulations

OFDM was selected in LTE/LTE-A due to its efficiency and simplicity using baseband modulation and demodulation stages based on Fast Fourier Transform (FFT). In a single carrier modulation system, the data is sent serially over the channel by modulation one single carrier at a baud rate of R symbols per second. The data symbol period is $T_{symbol} = \frac{1}{R}$. So the energy associated with each symbol is distributed over the entire bandwidth. In the frequency-domain, by applying the Fourier Transform (FT), the expression for the complex envelope of a N-symbol burst (N is considered an even value for reasons of simplicity) can be written as:

$$S(f) = \mathfrak{F}\{s(t)\} = \sum_{k=0}^{N-1} s_n R(f) e^{-j\pi f n T_s} \tag{3.2}$$

Where s_n is a complex coefficient corresponding to the nth symbol determined from a certain constellation (for example QPSK), T_s is the symbol duration and $R(f)$ is the Fourier Transform of the transmitted impulse.

In a multicarrier transmission, the data signal is divided into several different sub-streams that are sent via different sub-channels. The available bandwidth, B, is divided into a number N_c of sub-bands, called subcarries. The spacing between subcarriers is

$$\Delta f_c = \frac{B}{N_c} \tag{3.3}$$

Instead of transmitting the data symbols in a serial way at a baud rate R, a multicarrier transmitter sends the data stream into blocks of N_c data symbols and those are transmitted in parallel by modulating the N_c subcarriers. The symbol duration for a multicarrier scheme is $T_{symbol} = \frac{N_c}{R}$ [32].

Multicarrier modulations are characterized by the transmission of information in the frequency-domain according to the following expression:

$$S(f) = \sum_{k=0}^{N-1} S_k R(f - kF) \tag{3.4}$$

F represents the spacing between the subcarriers and the S_k symbolizes the kth symbol in the frequency-domain.

The FFT and Inverse Fast Fourier Transform (IFFT) are two mathematical tools used in the receiver and transmitter part of the OFDM, respectively.

Applying the inverse FT the following expression is obtained:

$$s(t) = \mathfrak{F}^{-1}\{S(f)\} = \sum_{k=0}^{N-1} S_k r(t) e^{-j2\pi k F t} \tag{3.5}$$

For the impulses of $r(t)$ to be orthogonal, and so, to avoid ISI (intersymbol interference), this condition must be followed:

$$\int_{-\infty}^{+\infty} r(t - nT_s)r^*(t - n'T_s)dt = 0, n \neq n' \tag{3.6}$$

3.4 SubCarrier Spacing

4G LTE supports inter-subcarrier spacing of 15 kHz with bandwidths up to 20 MHZ and a fixed OFDM numerology. There are exceptions, like NB-IOT defined in 3GPP Release 13 can support single-tone transmissions at 3.75 kHz subcarrier spacing [33]. 5G NR, subcarrier spacing index (μ) can have five possible values as specified in [34]. The subcarrier spacing is calculated by the numerology in the following way: $\Delta f = 15 \times 2^{\mu}$. For the range of μ values 0 through 4, this translates into subcarriers spacing of 15, 30, 60, 120 and 240 kHz, respectively and the correspondent maximum carrier bandwidths is 50 MHz, 100 MHz, 200 MHz and 400 MHz .

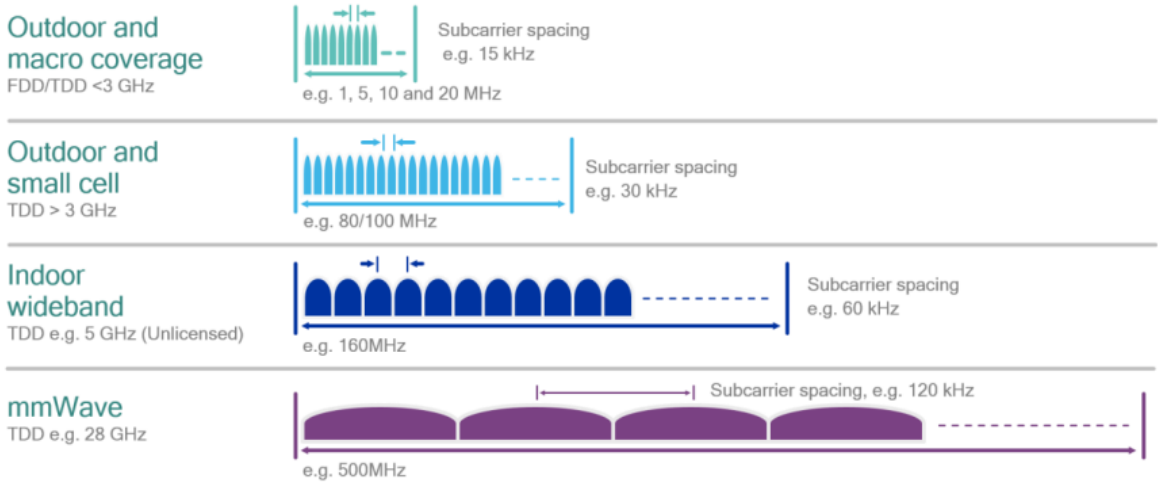

Figure 3.3: Example usage models, channel bandwidths, and subcarrier spacing [33]

3.5 Numerology and Scalability

As mentioned, OFDM plays a important paper in 5G NR, both in uplink and downlink. To reach all the specifications that are necessary in 5G, more than a single fixed OFDM numerology is needed. LTE supports carrier bandwidths up to 20 MHz with an known OFDM numerology, a fixed CP duration and a fixed subcarrier spacing as well. More precisely $4.69\mu s$ CP and a 15 kHz subcarrier spacing. On the other hand, NR, will support different numerologies, going from $\mu = 0$ until $\mu = 4$, who respectively correspond to subcarrier spacing from 15 to 240 kHz(see Table 3.1).

Table 3.1: Scalable OFDM numerology for 5G NR for all spectrum options [35]

Numerology (μ)	0	1	2	3	4
$\Delta f = 15 * 2^{\mu}$	15	30	60	120	240
Frequency Band (GHz)	0.45-6	0.45-6	0.45-6 24-52.6	24-52.6	24-52.6
Symbol duration (μs)	66.67	33.33	16.67	8.33	4.17
Cyclic Prefix Type	Normal	Normal	Normal/ Extended	Normal	Normal
Cyclic Prefix (μs)	4.69	2.34	1.17	0.59	0.29
Maximum bandwidth (MHz)	50	100	100	400	400
Slot duration (ms)	1.0	0.5	0.25	0.125	0.625
Number of symbols/slots	14	14	14 / 12	14	14
Number of slots/subframes	1	2	4	8	16

3.6 Cyclic Prefix

The inclusion of CP in OFDM makes it robust to timing synchronization errors. When OFDM signals are being transmitted in multipath fading channels, various copies of the transmitter signal can be received at slightly different time intervals, which can cause ISI. Therefore, passing the OFDM subcarriers through a time-dispersive channel, they can lose their orthogonality due to ISI, resulting in inter-carrier interference (ICI). The multiple signals that appear due to the multipath propagation arrive at the receiver at different times, spreading the symbol boundaries and causing interference between the OFDM symbols. Besides, the phase and amplitude of the subcarrier must remain constant over a period of the symbol in order to maintain the orthogonality . If they are no constant, the spectral shape will not have nulls at the correct frequencies [36]. This is ICI.

The solution for this problem passes by adding a guard period to the start of each symbol. This guard period, which is called the CP, Fig 3.4, is a copy of the last part of the OFDM symbol, thus extending the length of the symbol waveform. The inclusion of the CP adds redundancy to the transmission since the same content is transmitted twice as the CP is a copy of the tail of a symbol placed at its beginning [37].

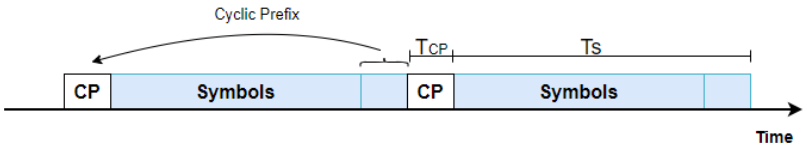

Figure 3.4: Cyclic Prefix implementation

For LTE, a choice of a cyclic prefix of 4.7μs with subcarriers spaced by 15 kHz, offers

a good balance for scenarios with wide-area deployments using lower-frequency spectrum, scenarios for witch LTE was originally designed. 5G NR, is designed to support a wide range of deployment scenarios with very wide spectrum allocations. Having a single numerology for all these scenarios is not efficient or even possible. So, in NR, the prefix is composed of the last N_{CP} samples of the symbol, the CP length for different subcarrier is given by [34] :

$$N_{CP} = \begin{cases} 512k \times 2^{-\mu}, & extended \quad cyclic \quad prefix \\ 144k \times 2^{-\mu} + 16k, & normal \quad cyclic \quad prefix, \quad l = 0 \quad \vee \quad l = 7 + 2^{-\mu} \\ 144k \times 2^{-\mu}, & normal \quad cyclic \quad prefix, \quad l \neq 0 \quad \vee \quad l \neq 7 + 2^{-\mu} \end{cases} \tag{3.7}$$

, k is a constant that represents the ratio between NR basic time unit and LTE basic time unit and can be represented by the following expression :

$$k = \frac{T_s}{T_c} = 64 \tag{3.8}$$

, and CP time duration is given by :

$$T_{CP} = N_{CPc} \tag{3.9}$$

Table 3.2: Cyclic prefix OFDM Symbol Duration for 5G NR [34]

Numerology (μ)	**Subcarrier Spacing (kHz)**	**OFDM symbol duration** $T_s(\mu s)$	**Cyclic Prefix** $T_{cp}(\mu s)$	**Cyclic Prefix Long Symbol** (μs)
0	15	66.7	NCP = 4.69	l=0 or 7 NCP= 5.2
1	30	33.3	NCP = 2.34	l=0 or 14 NCP= 2.86
2	60	16.7	NCP = 1.17 ECP = 4.17	l=0 or 28 NCP= 1.69 ECP= 4.17
3	120	8.33	NCP = 0.59	l=0 or 56 NCP= 1.11
4	240	4.17	NCP = 0.29	l=0 or 112 NCP= 0.81

Watching the Table 3.2, we can conclude that as the subcarrier spacing increases, the cyclic prefix length decreases, resulting in more susceptibility of NR signals to multipath delay distortion and coverage reduction, increasing then, the NR signal tolerance to Doppler shift. For below 7.125 GHZ bands (FR1), smaller subcarrier spacing must be used, while the higher subcarrier spacing are intended for above 24 GHz (FR2) due to the better tolerance for phase noise with higher frequency bands [1]. The normal CP is supported for all subcarrier spacing values, whereas extended CP is only supported for μ=2.

3.7 Generic Frame Structure

5G NR air interface resources are allocated in frames of 10 ms duration, like 4G LTE, regardless of the numerology used. Each frame is divided of 10 subframes with 1 ms duration each (Figure 3.5). The $1ms$ subframe is then divided into one or more slots in 5G, while LTE has exactly two slots in a subframe. Because LTE uses a SCS of 15 kHz, the first numerology of $\mu = 0$, which has the same subcarrier spacing, will have its slots with an identical structure to facilitate coexistence with both generations. Different numerologies will then translate

into the number of slots per subframe. So, the higher the subcarrier spacing, the higher the number of slots per sub-Frame. The slot length in millisecond is defined as : Slot Length $=\frac{1}{2^{\mu}}$

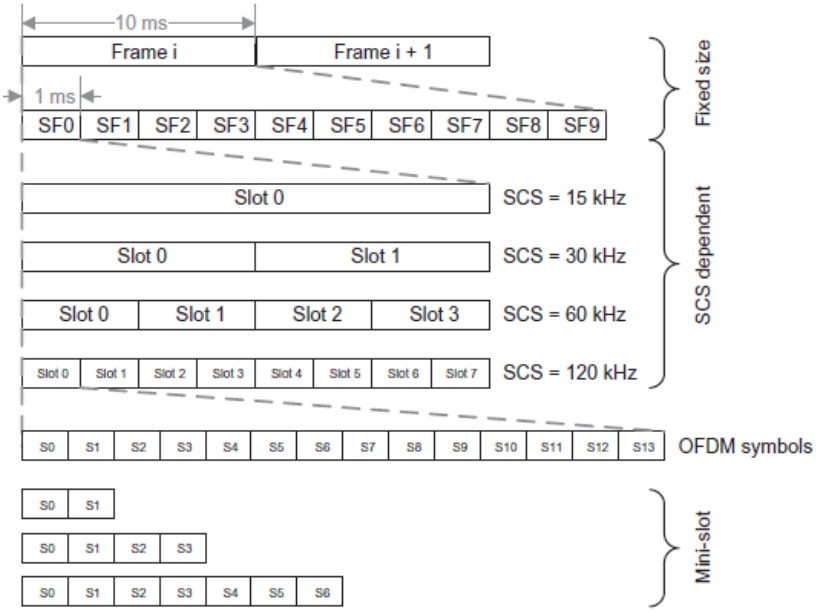

Figure 3.5: 3GPP NR frame structure [34]

The frame structure provides the basis for the timing of physical signal transmission. Each slots consists of 14 OFDM symbols in the time domain and 12 subcarriers in the frequency domain. An exception to this is the 60 kHz subcarrier spacing with an extended CP. In this case, each slot consists of 12 OFDM symbols in the time domain. The extended CP is used when it is needed to reduce the slot duration and delay while maintaining a CP similar to 15 kHz.

5G NR also supports mini slot concept. Mini slots can be used to support shorter transmissions, since a mini-slot can be as short as one OFDM symbol in time. The purpose of the mini slot is to enable low latency communication for all subcarrier spacings. Because of the flexible time structure of the mini-slots, they can be used in scenarios where the transmission needs to start immediately. In addition it is possible to schedule data using a mini-slot with a length of typically 2, 4, or 7 symbols, where the first symbol includes (uplink or downlink) control information [38].

Slot format indicates how each slot will use the symbols. A symbol can be used for downlink , uplink or can be flexible. Unlike in LTE , where a subframe (equivalent to a slot in NR) was either configured for DL or UL, all number of symbols within the subframe had to be use as DL or UL. In NR, this is not the case since in a given slot each symbol can be configured in various ways. Theoretically we can have a infinite number of possible combinations, but 3GPP [39] allows only 61 predefined symbol combination within a slot. In the table 3.3, are some examples of configurations defined by 3GPP technical report.

Table 3.3: Slot formats for normal prefix [39]

D : Downlink , U: Uplink , F: Flexible

	Symbol Number in a slot													
Format	0	1	2	3	4	5	6	7	8	9	10	11	12	13
0	D	D	D	D	D	D	D	D	D	D	D	D	D	D
1	U	U	U	U	U	U	U	U	U	U	U	U	U	U
2	F	F	F	F	F	F	F	F	F	F	F	F	F	F
7	D	D	D	D	D	D	D	D	D	F	F	F	F	F
15	F	F	F	F	F	F	U	U	U	U	U	U	U	U
32	D	D	D	D	D	D	D	D	D	D	F	F	U	U
55	D	D	F	F	F	U	U	U	D	D	D	D	D	D
62-254	Reserved													
255	UE determines the slot format													

3.8 Resource Element, Resource Grid and Resource Blocks

- **Resource element** is the smallest physical resource in NR. It consists of one subcarrier in the frequency domain and of one OFDM symbol in the time domain, is the same as LTE.
- **Resource Block** in NR, is defined only for frequency domain. 12 consecutive subcarriers constitute a RB. The difference between LTE and 5G is that, in LTE a resource block bandwidth is fixed to 180 kHz but in NR it is not fixed and depend on sub-carrier spacing.
- **Point A** is a reference point to locate the resource blocks in a given carrier and functions as a reference point to describe all resource grids in the frequency domain. It will be located in the first subcarrier of the first common resource block, for all subcarrier spacings.
- **Common Resource Blocks (CRB)** are numbered differently according to each numerology, and go from 0 till max RB supported for a given subcarrier μ. For each numerology, the starting point of its transmission bandwidth configuration on the CRB grid for a given channel bandwidth is indicated by an offset to reference point A [38].

  The relation between the common resource block number n^{μ}_{CRB} in the frequency domain and resource elements, for subcarrier spacing configuration μ is given by the following expression, [34]

$$n^{\mu}_{CRB} = \left[\frac{k}{N^{RB}_{sc}}\right] \tag{3.10}$$

  where k is defined relative to point A such that k = 0 corresponds to the subcarrier centered around point A.
- **Physical Resource Blocks (PRB)** are defined in a given Bandwidth Part (BWP) as PRB, and will be numbered from 0 to $N^{size}_{BWP,i} - 1$, where i is the BWP number. The relation between PRB and the CRB is given by [34]:

$$n^{\mu}_{CRB} = n^{\mu}_{PRB} + N^{start}_{BWP,i} \tag{3.11}$$

, where $N^{start}_{BWP,i}$ is the CRB where the BWP starts relative to CRB 0. PRB boundaries corresponding to different numerologies are frequency aligned relative to a Point A, fig 3.6 .

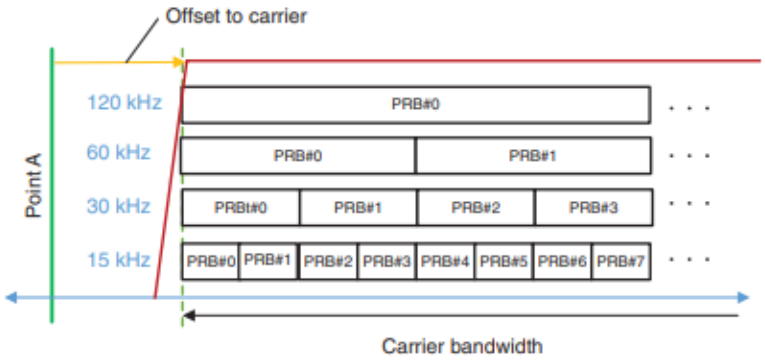

Figure 3.6: PRB alignment for different numerologies [40]

- **Virtual Resource Blocks (VRB)** are defined within a BWP and are enumerated from 0 to $N^{size}_{BWP,i} - 1$, similar to LTE [34]. The virtual resource blocks are resource blocks that are permuted across frequency dimension to take advantage of frequency diversity.
- **Resource Grid** for NR is illustrated as the figure 3.7.

  While for $\mu = 0$ it is similar to LTE, the physical dimension (subcarrier spacing, number of OFDM symbols), varies in NR according to higher numerologies. For a given antenna port p, numerology on the same carrier and transmission direction (downlink or uplink) there will be a different resource grid. An antenna port is a logical entity which is different from a physical antenna concept. Each p is associated with a specific set of reference signals such that the channel over which a symbol is conveyed can be inferred from the channel over which another symbol on the same antenna port is conveyed [34]. Each RG will have $N^{size,\mu}_{grid,x} \times N^{RB}_{sc}$ subcarriers and $N^{subframe,\mu}_{symb}$ OFDM symbols. From the figure 3.7, we can also conclude that each resource element in the resource grid is identified by pair (k, l), where k is the index in the frequency domain and l is the symbol position in the time domain.

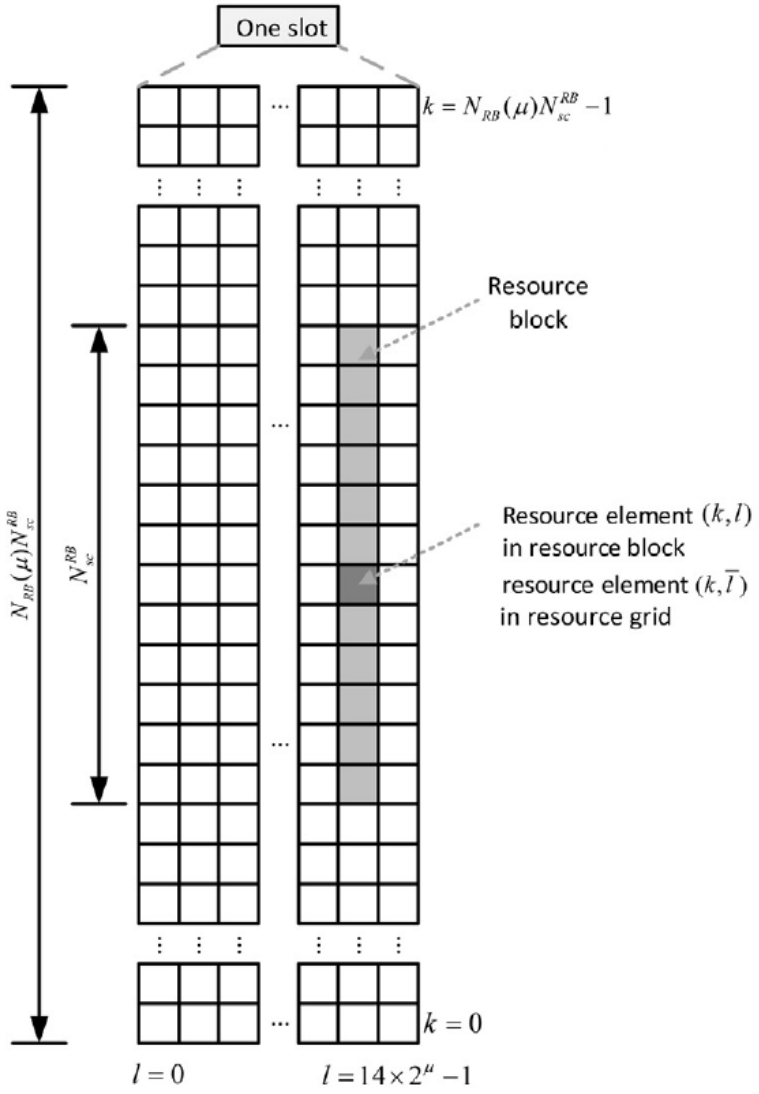

Figure 3.7: Illustration of resource grids supported by NR [38]

3.9 Channel Bandwidth

An NR system supports much wider maximum bandwith than LTE 20 MHz. In NR, the channel bandwith was implemented in order to support ranges from 5 to 400 MHZ. One or more RB form a UE channel bandwidth or transmission bandwidth, so we can say that the limit of the spectrum will be specified by the maximum number of physical RB (see Fig 3.8). The guard band added at the edges of each carrier it will depend on the numerology used. For a channel bandwidth the guard band will be given by the following expression [1]:

$$W_{guard} = \frac{BW_{Channel} - N_{RB} * 12 * \Delta f - \Delta f}{2} \tag{3.12}$$

being N_{RB} the maximum number of resources blocks possible and Δf is the subcarrier spacing.

Each numerology has defined minimum and maximum number of resource block and having knowledge of one resource block bandwidth one can calculate minimum and maximum channel bandwidth. Compared to LTE, 5G NR is designed to have higher bandwidth efficiency, reaching 98 %, compared to 90 in LTE, where 100 RB covered only 18 MHz in a 20 MHz Bandwidth carrier.

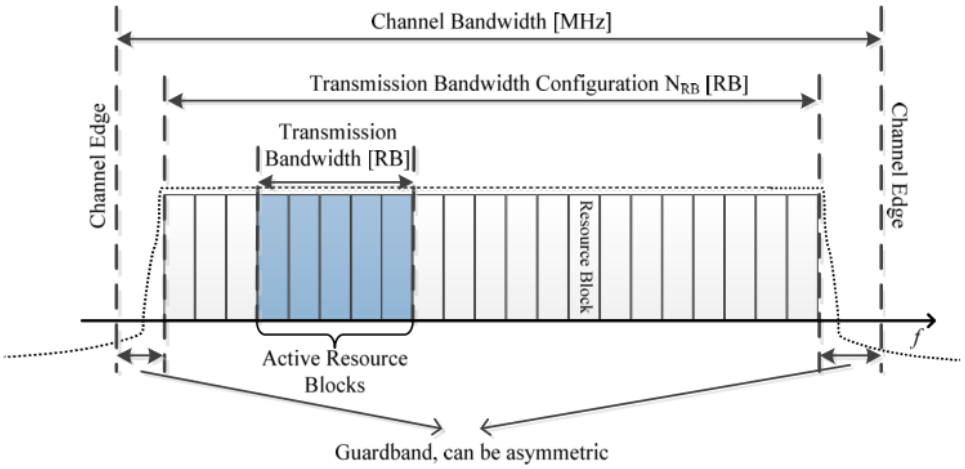

Figure 3.8: Definition of channel bandwidth and transmission bandwidth configuration for one NR channel [28]

Table 3.4: Transmission bandwidth configuration for FR1 [28]

SCS (kHz)	**5 MHz**	**10 MHz**	**15 MHz**	**20 MHz**	**25 MHz**	**30 MHz**	**40 MHz**	**50 MHz**	**60 MHz**	**70 MHz**	**80 MHz**	**90 MHz**	**100 MHz**
	NRB	**NRB**	**NRB**	**NRB**	**NRB**	**NRB**	**NRB**	**NRB**	**NRB**	**NRB**	**NRB**	**NRB**	**NRB**
15	25	52	79	106	133	160	216	270	N/A	N/A	N/A	N/A	N/A
30	11	24	38	51	65	78	106	133	162	189	217	245	273
60	N/A	11	18	24	31	38	51	65	79	93	107	121	135

Table 3.5: Transmission bandwidth configuration for FR2 [28]

SCS (kHz)	**50 MHz**	**100 MHz**	**200 MHz**	**400 MHz**
	N_{RB}	N_{RB}	N_{RB}	N_{RB}
60	66	132	264	NA
120	32	66	132	264

The tables 3.4 and 3.5 summarises the relation between the $BW_{Channel}$ and the corresponding maximum N_{RB}. The OFDM can be implemented using FFT/IFFT blocks at the receiver/transmitter. As such the FFT is a crucial element of these systems, is important to know is size. The FFT size can be related with the sampling frequency by the following expression :

$$F_s^{\mu} = \Delta_f^{\mu} \times N_c^{\mu}, \quad \mu \in \{0, 1, ...4\} \tag{3.13}$$

where Δ_f^{μ} is the frequency subcarrier spacing and N_{FFT}^{μ} is the total number of subcarriers (FFT/IFFT size).

To find the data number of occupied subcarriers N_d^{μ}, we can use the relation $N_d^{\mu} = 12 \times N_{rb}$, where the number of available physical resource blocks N_{rb} can be found in the tables 3.4 and 3.5.

The sampling frequency for each case scenario is present on tables A.1, A.2, A.3 and A.4 (see Appendix A).

CHAPTER 4

Linear equalization for discrete Fourier transform-spread-OFDM (DFT-s-OFDM)

This chapter aims to provide a complete picture of the single-carrier transmission technique DFT-s-OFDM. The Chapter is organized in two parts. In the first part we present principles/characteristics of DFT-S-OFDM technique, like transmitter/receiver structure, and in the second part we study the impact of the linear equalization for the different 5G numerologies. The goal of equalization is to compensate the effects of channel distortion due to frequency selectivity.

4.1 DFT-s-OFDM Structure

The orthogonal frequency-division multiplexing (OFDM) technique has been widely adopted to cope with the frequency-selective fading of multipath channels in wireless communications. The transmit signals in an OFDM system can have high peak values in the time domain since many subcarrier components are added via an IFFT operation, one of this high peak values its the peak-to-average power ratio (PAPR), which decreases the Signal-to-Quantization Noise Ratio (SQNR) of Analog-to-Digital Converter (ADC) and Digital-to-Analog Converter (DAC), raising the cost and lowering the power efficiency of the transmitter power amplifier. The PAPR problem is more important in the uplink since the efficiency of the power amplifier is critical due to the limited battery power in a mobile terminal.

A principal motivation for adopting DFT-s-OFDM, (Figure 4.1), in 5G NR cellular systems is the fact that its PAPR is lower than that of alternative transmission techniques. So, one of the multiple access technique selected to be used in the UL of 5G NR, was the DFT-s-OFDM.

Comparing with an OFDM system where a DFT-spread block is not employed and the symbols are mapped to the subcarriers directly, in DFT-s-OFDM, the data symbols are first spread with a DFT block, and then mapped to the input of an IDFT block. From figure 4.2,

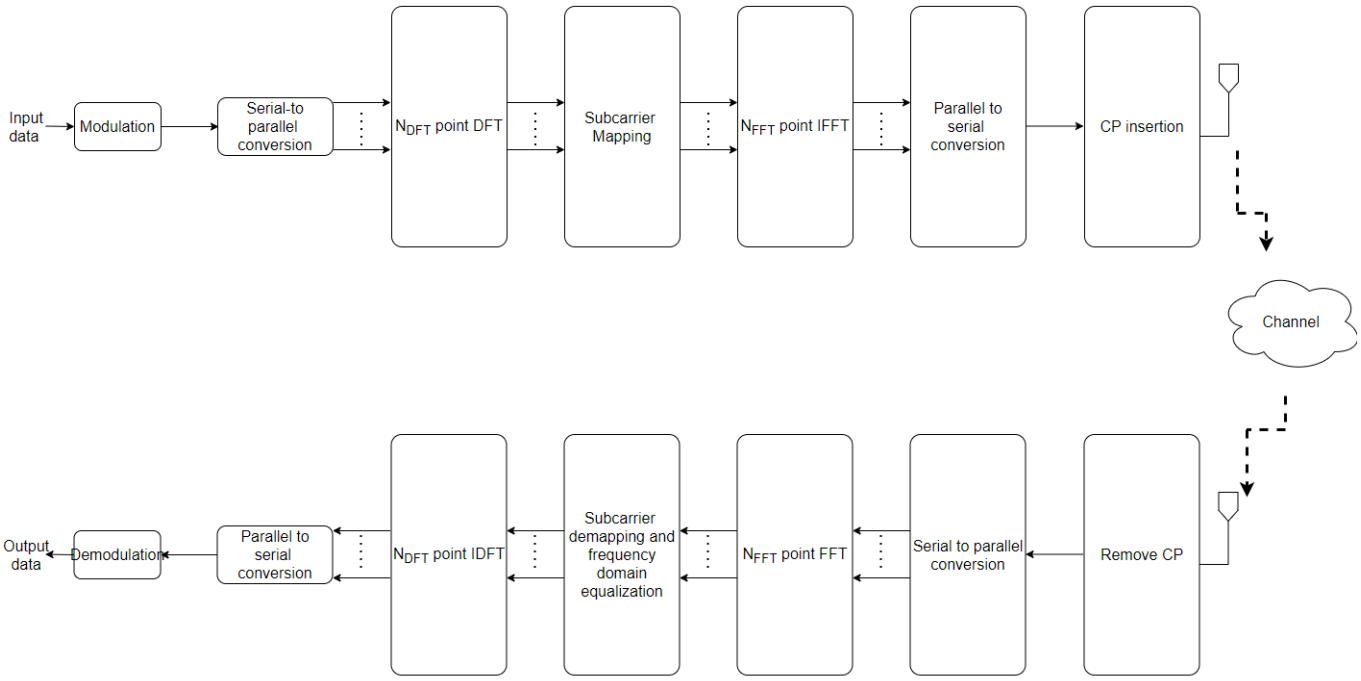

Figure 4.1: A block diagram of a DFT-spread OFDM system (note that $N_{DFT} < N_{FFT}$)

we can observe the comparison of 4 QPSK data symbols transmitted using a OFDM and DFT-s-OFDM.

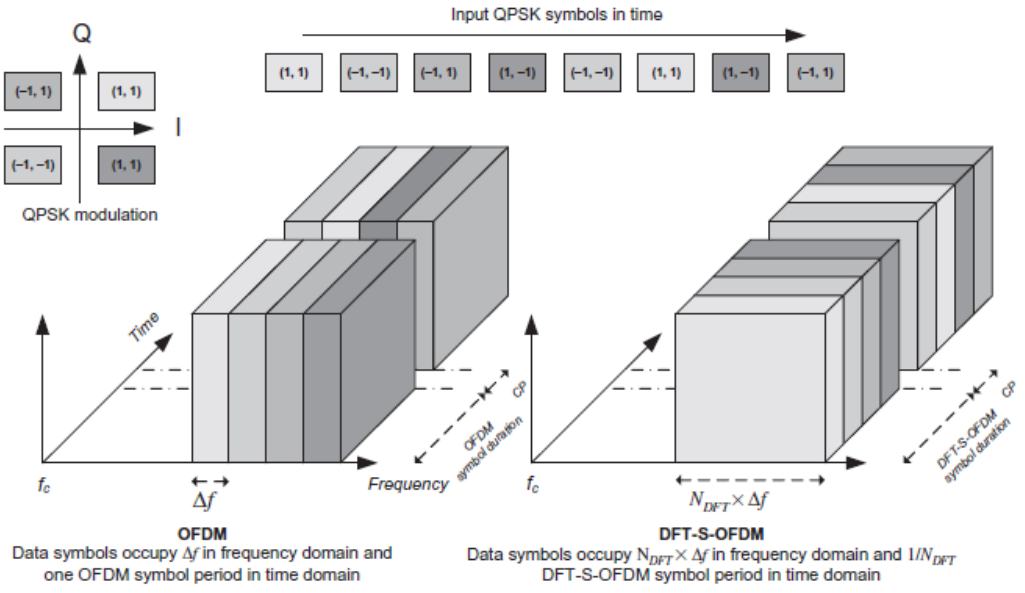

Figure 4.2: Comparison between OFDM and DFT-s-OFDM [38]

For OFDM, each symbol period transmits 4 QPSK data symbols in parallel, each of them modulating its own subcarrier at the appropriate QPSK phase. After a symbol period, a CP is inserted to mitigate the multipath effects. In the DFT-s-OFDM each symbol also transmits

4 QPSK data symbols, but each symbol is transmitted sequentially and spreaded over the 4 subcarriers. Therefore, each DFT-s-OFDM symbol occupies $N_{DFT} \times \Delta f$ bandwidth, assuming a subcarrier spacing of Δf. After 4 QPSK data symbols a CP is inserted, so we can conclude that OFDM and DFT-s-OFDM periods are the same.

4.2 Transmission and Receiver chain

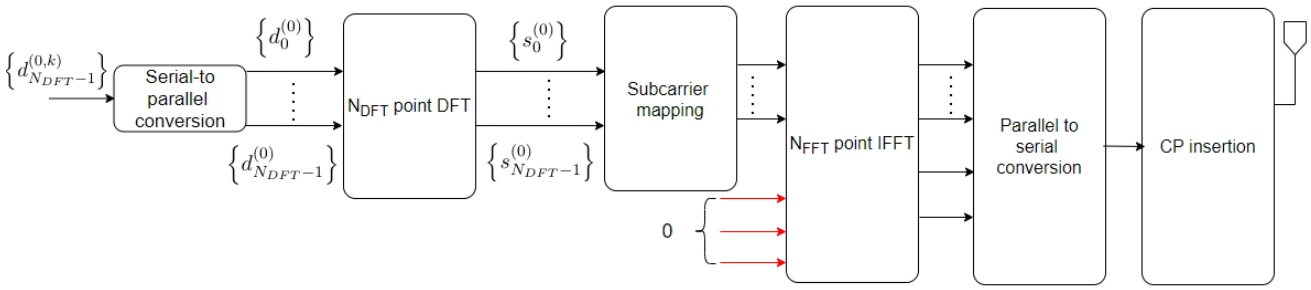

Figure 4.3: DFT-spread OFDM transmitter block diagram (note that $N_{DFT} < N_{FFT}$)

As for the implementation, lets assume a set of users that transmit N_{DFT} data symbols on different resources to the base station, at the user transmitter side (Figure 4.3). Initially the data is QPSK baseband modulated. Hereafter, a DFT operation is made. Because the data input can be modeled as independent and identically distributed random variables, and as a result, the corresponding output of IDFT is going to have high variance that is reduced by providing correlation to the input data by performing a DFT operation before the IDFT process [41]. After the N_{DFT}-point DFT for a set of N_{DFT} data symbols, are converted into frequency domain.

Similar to LTE , in NR, the N-point DFT size is restricted to products of the integers two, three and five. Ideally the DFT size should be constrained a power of 2 because of implementation complexity reasons but such limitation would limit the scheduler flexibility in terms of the amount of resources that can be assigned for an uplink transmission. In this way, the DFT can be implemented following the relation:

$$N_{DFT} = 2^{a_2} \times 3^{a_3} \times 5^{a_5} \tag{4.1}$$

It is important to notice that the uplink resource attribution is always done in terms of resource blocks of size 12 subcarriers, so the DFT size has the particularity of being a multiple of 12 . For example sizes of 60, 72 and 96 are allowed, but a DFT size of 84 is not allowed. In our case is going to be use DFT size of 96 data symbols.

Figure 4.4 shows the user mapping after the DFT operation. The data transmitted of each user are distributed over 96 subcarriers and mapped on adjacent positions. Following the subcarrier mapping a N_{FFT}-point IFFT operation is made, converting the subcarrier signals to time domain. As mentioned, a set of each users are transmitted in different set of carriers

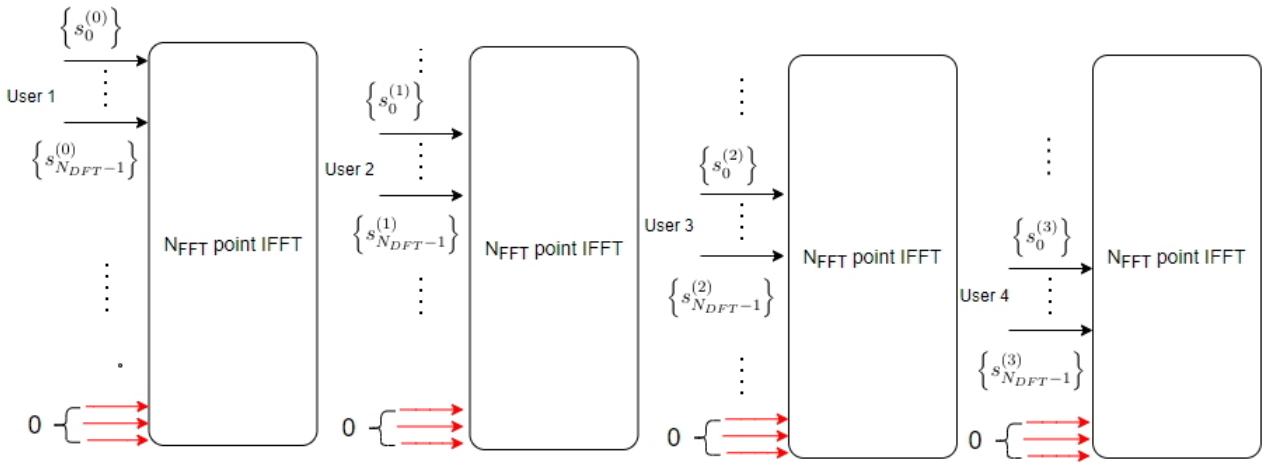

Figure 4.4: Users mapping before the IFFT operation

making sure there is no multi-user interference in the system. In order to improve the BER results , because of the TDL models channels have a low selective frequency response diversity, the users data symbols that occupy a set of subcarriers are going to be distributed over the entire frequency range of the channel increasing the frequency diversity order [42]. So, for the different users the data information is going to be spread in the bandwidth by a factor S, with a equi-distance of $S = \frac{N}{M}$, where N is the number of subcarriers available (N_{FFT}) and M is the number of consecutive subcarriers used for each user (N_{DFT}).

The transmitter performs other signal processing operations previous to transmission. It inserts the CP in order to implement a guard time to avoid ISI, due to multipath propagation. As mentioned in 3.6, the CP is a copy of the last fraction of the most recent block, which is added to the beginning of the next block.

The ith transmitted symbol in the frequency domain at single transmit/receive antenna case can be expressed, before the IDFT, as a vector of length N_{FFT} defined by $\mathbf{y}=\mathbf{F\Theta Dd}$, where $\mathbf{d}=[d_1\ d_2\ ...\ d_N]^T$ is an $N_{DFT} \times 1$ vector with N_{DFT} QAM-modulated symbols (T represents the transpose operation), $\mathbf{D}$ represents the DFT matrix of size $N_{DFT} \times N_{DFT}$, $\mathbf{\Theta}$ is the $N_{FFT} \times N_{DFT}$ mapping matrix for subcarrier assignment and $\mathbf{F}$ performs N_{FFT}-point IFFT operation.

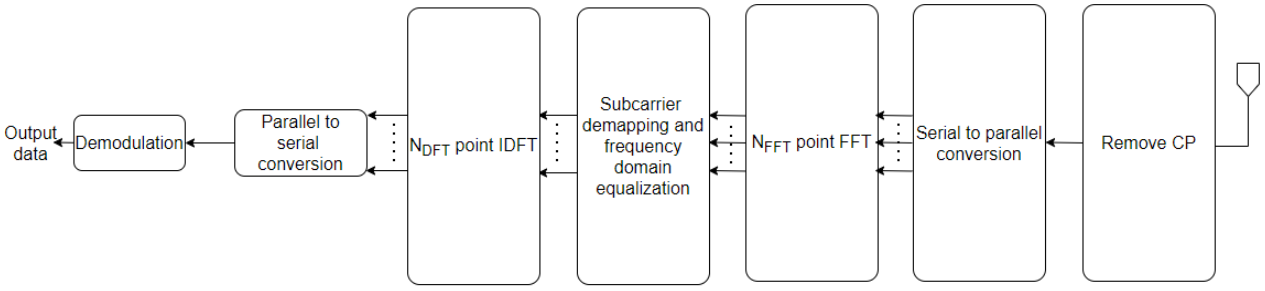

Figure 4.5: DFT-spread OFDM receiver block diagram

In the receive side chain, (Figure 4.5), the inverse operations are performed. Firstly the CP is removed, then, the $N_{FFT}-$point FFT is applied to convert the signal to frequency domain. Following, the subcarriers, correspondents to each user, are de-mapped and equalization is performed in the frequency domain (see Figure 4.6), as alternative to a time-domain equalization, significantly reducing the complexity of linear equalization. The objective of equalization is to compensate the effects of the multipath channel and to restore the original signal. At the end of the receiver chain, the equalized signal is converted back into time domain by an IDFT block.

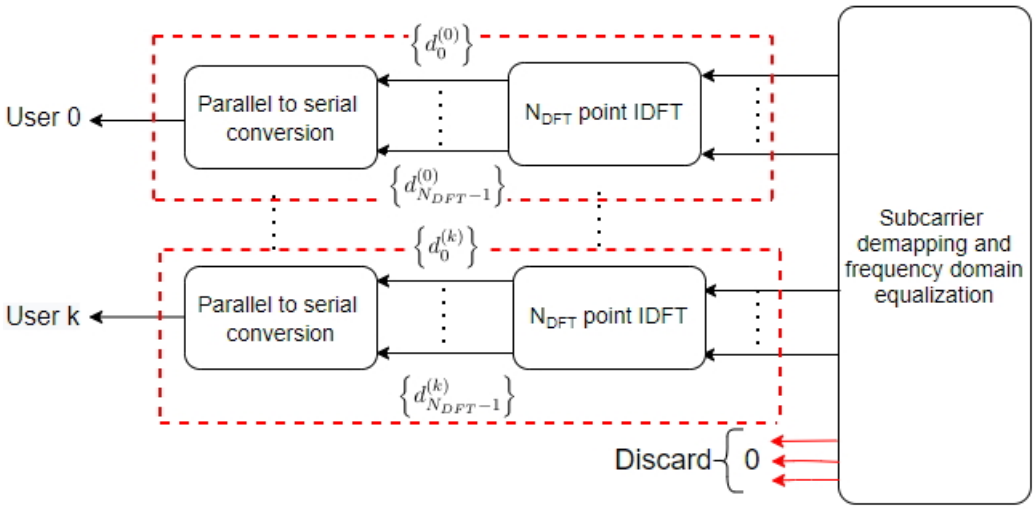

Figure 4.6: Users demapping with respective equalization

After the propagation through the multipath fading channel, addition of the AWGN, removing the CP and going through the N_{FFT}-point FFT process, the received signal vector in frequency domain is, $\hat{\boldsymbol{z}}$=$\mathbf{H\Theta Dd+n}$, where $\mathbf{H}$ is the diagonal matrix of channel response and $\mathbf{n}$ is the noise vector. The amplitude and phase distortion in the received signal due to the multipath channel is compensated by a frequency-domain equalizer. The estimated signal after equalization processing can be expressed as $\hat{\boldsymbol{z}}$=$\mathbf{GH\Theta Dd+Gn}$, with $\mathbf{G}$ being the diagonal matrix of equalizer coefficients.

After the subcarrier demapping function and IDFT despreading a vector $\hat{\mathbf{s}}$, contains the receiver N_{DFT} QAM-modulated symbols as an estimate to the input vector $\mathbf{d}$. Therefore, the estimated symbols, $\hat{\mathbf{s}}$, after the IFFT operation are given by, $\hat{\mathbf{s}}$=$\mathbf{D}^{-1}\mathbf{GHDd + nG}$.

We can conclude that the estimated symbol vector is perfectly estimated at the receiver if $\mathbf{GH=I}$. For this to happen we need to use equalizers, to remove or minimize the channel's effect and the noise, that's why they are so important on system performance.

4.3 Equalization Schemes used in SISO DFT-s-OFDM system

If the channel was noiseless and flat, the OFDM signal would be received without errors, however the channel is noisy and has multipath effect. Another important aspect, already mentioned, is the fact that the IDFT despreading makes DFT-s-OFDM more sensitive to

the noise, because the IDFT block in the receiver averages the noise over each subcarrier. Thus, equalization needs to be performed in order to obtain, the correct estimated QAM-modulated symbols data, at the receiver. The different equalizers generally used in this systems and used considered in this work are the Maximum Ration Combining (MRC), Equal Gain Combining (EGC), Zero Force Combining (ZFC) and Minimum Mean Square Error Combining (MMSEC). In the frequency domain the different types of equalizers, with N_{FFT} channel coefficients and k the k-th data symbol, are given by :

- Maximum Ratio Combining:

$$MRC: \quad g_k = h_k^* \qquad , k = 1, ..., N_{FFT} \tag{4.2}$$

  The principal objective of MRC equalization is to maximize the instantaneous SNR at the receiver. This equalizer have good results for AWGN channels because the signal is multiplied by a weight factor proportional to the signal amplitude. The coefficients are acquired simply from the complex conjugate of the frequency response of the channel. This equalization scheme does not restore orthogonality to the detected signal and so, any variation in the channel coefficient can cause ICI [43].

- Equal Gain Combining:

$$EGC: \quad g_k = \frac{h_k^*}{|h_k^*|} \qquad , k = 1, ..., N_{FFT} \tag{4.3}$$

  In this method, the coefficients tries to compensate the effects of the phase rotation caused by the channel. The orthogonality, in this case, is also not restored [43].

- Zero Forcing Combining:

$$ZFC: \quad g_k = \frac{h_k^*}{|h_k^*|^2} \qquad , k = 1, ..., N_{FFT} \tag{4.4}$$

  The ZFC criteria recovers the orthogonality, unlike the previous methods, forcing the ISI to zero. The ZFC is a linear equalization which applies the inverse of the frequency response of the channel to the received signal. As disadvantage this equalizer amplifies the noise term when channel coefficients have low amplitude [44].

- Minimum Mean Square Error Combining:

$$MMSEC: \quad g_k = \frac{h_k^*}{|h_k^*|^2 + \sigma^2} \qquad , k = 1, ..., N_{FFT} \tag{4.5}$$

  where σ^2 is the noise variance. The MMSEC takes care of the noise amplification because the coefficients are optimized with the minimum mean squared error. In this technique there will be a necessity of having a trade-off between noise enhancement and inter-carrier interference [44].

4.4 **Numerical results**

In this section, we present and discuss the main simulation results obtained for the discussed linear equalizers considering the parameters presented in table 4.1. The results obtained for different channels and numerologies in the 5G NR, are presented in term of average BER as function of $\frac{E_b}{N_0}$.

Table 4.1: DFT-s-OFDM parameters used in BER performance simulations

Parameters		**Values**			
Subcarrier separation (Δf) (kHz)		15	30	60	120
Channel Bandwidth (MHz)		25	50	100	200
FFT Size		2048	2048	2048	2048
CP size (μs)		144	144	144	144
Sampling Frequency (MHz)		30.72	61.44	122.88	245.76
Number of available subcarriers		384	384	384	384
Delay Spread (ns)	TDL-A	30			
	TDL-B	100			
	TDL-C	300			
Modulation		QPSK			

Figure 4.7 shows the performance results for TDL-A channel under different numerologies. We also obtained results for all equalizers discussed above, MRC, EGC, ZFC and MMSEC. From the results it can be seen that the worst equalizing methods are the MRC and EGC. This happens because these equalizers do not restore the subcarriers orthogonality so the data cannot be recovered in the receiver without ISI. However, with the ZFC method it is possible to recover the recover the orthogonality but on the other hand this method enhances the noise, increasing BER. The most efficient equalizer is the MMSEC, since this method is a trade-off between the noise enhancement and the interference mitigation. Comparing now the results obtained for different subcarriers separation, we can see that the performance improves as the separation increases. This happens because increasing the carrier separation (the bandwidth is also increased, see Table 4.1) the channel becomes more selective in frequency domain (more number of paths are resoluble at the receiver) and thus the inherent diversity order is higher leading to performance improvement. The performance improvement is more significant for the MMSEC because this one is able to restore the orthogonality and thus can take all benefits of the additional added frequency diversity. Contrarily, the EGC and MRC equalizers are dominated by the interference and thus cannot take any advantage of the additional frequency diversity .

In figure 5.4, we obtained the results for different channel models TDL-A, B and C considering the same carrier separation of 15 kHz. It can be observed that the performance improves from the TDL-A to TDL-C. This is because the frequency selectivity of the channels

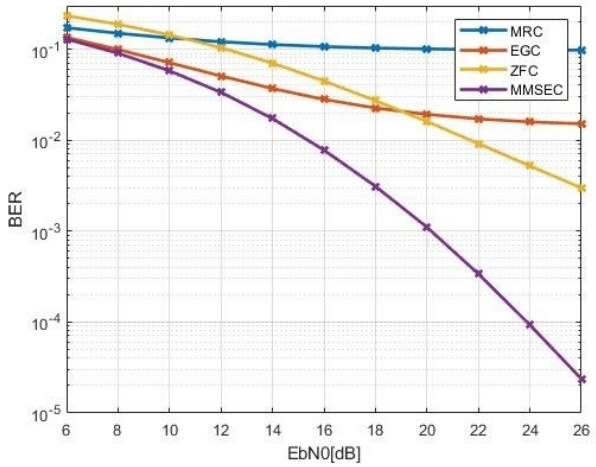

(a) Subcarrier spacing 15 kHz, TDL-A

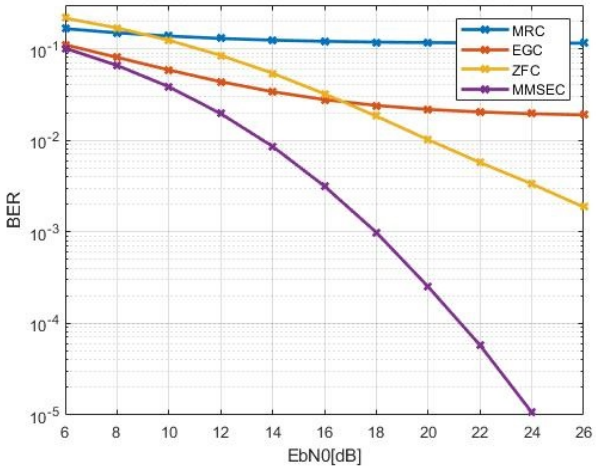

(b) Subcarrier spacing 30 kHz, TDL-A

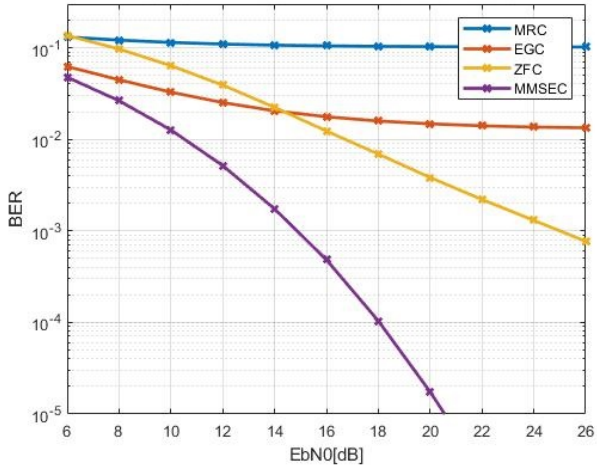

(c) Subcarrier spacing 60 kHz, TDL-A

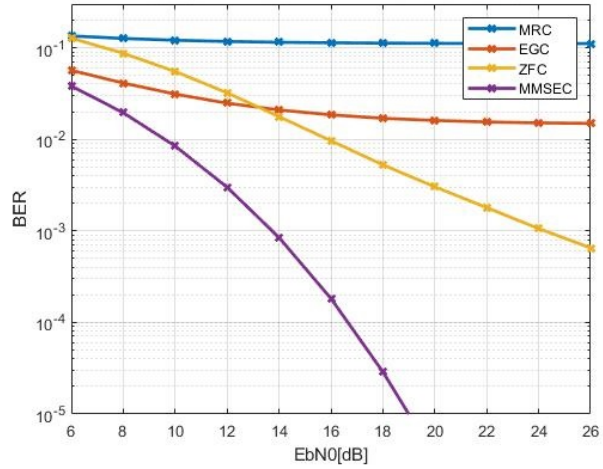

(d) Subcarrier spacing 120 kHz, TDL-A

Figure 4.7: BER performance of DFT-s-OFDM equalizers on SISO configuration

increases from TDL-A to TDL-C and thus the diversity order also increases leading to better performance as explained above.

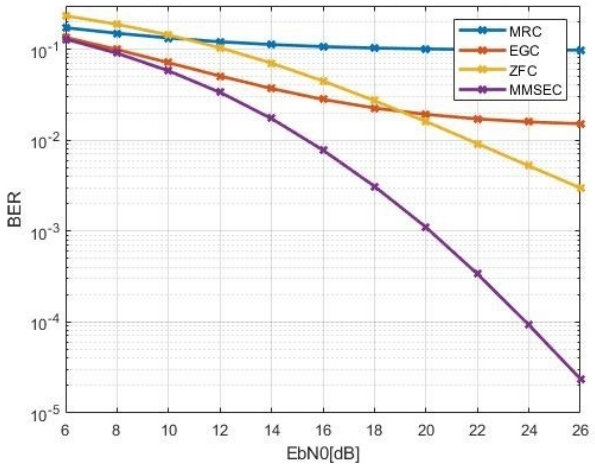

(a) Subcarrier spacing 15 kHz, TDL-A

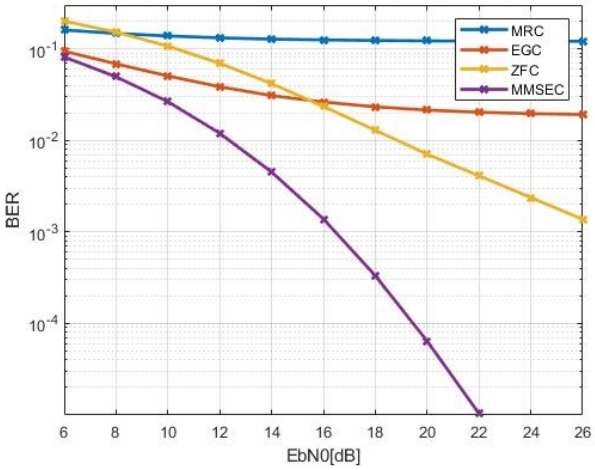

(b) Subcarrier spacing 15 kHz, TDL-B

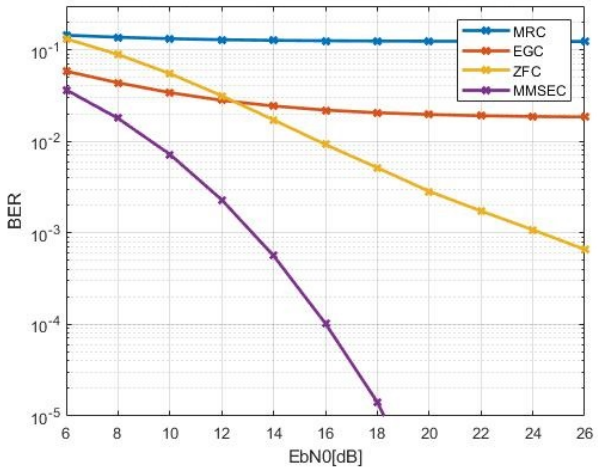

(c) Subcarrier spacing 15 kHz, TDL-C

Figure 4.8: BER performance for different TDL channels profiles with subcarrier separation 15 kHz

4.5 SIMO

Lets now consider the case where the receiver is equipped with multiple antennas. These systems can achieve space diversity in order to improve the transmission efficiency with no need to increase the bandwidth or additional power of transmission. Basically, diversity means that the information flows through different independent paths and this is a key element for a good use of inherent diversity in wireless channels and a consequent increase system reliability. The idea is to combine the different paths in order to mitigate the fading effects, since multiple independent paths are unlikely to fade simultaneously.

It is assumed that we have L receiver antennas. The received block associated to the lth antenna, after the DFT operation is given by,

$$y_{k,l} = s_k h_{k,l} + n_{k,l} \tag{4.6}$$

where $h_{k,l}$ represents the frequency domain channel response of the kth sub-carrier and $n_{k,l}$,

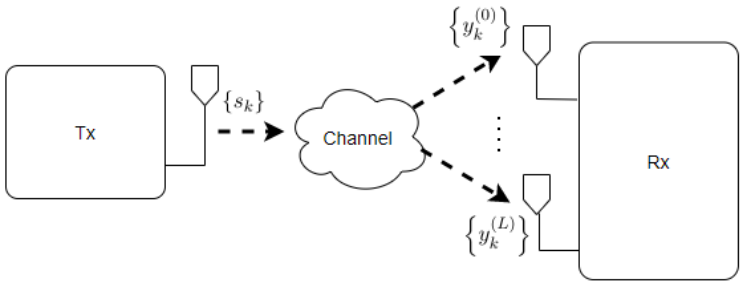

Figure 4.9: SIMO configuration

represents the noise at the carrier k. Comparing with the Single-Input Single-Output (SISO) system we can say that the estimated signal received in this case, is equivalent to the sum of the signal from two SISO systems with equivalent channels. Therefore, the estimated signal at the receiver is given by,

$$\hat{s}_{k,l} = \sum_{l=1}^{L} g_{k,l} y_{k,l} \quad , l = 1, ..., L, \quad k = 1, ..., N_{FFT} \tag{4.7}$$

, where $g_{k,l}$ is the equalization coefficient at subcarrier k and antenna l. The equalization coefficients used in this case, can be written by,

- Maximum Ratio Combining (MRC):

$$MRC: \quad g_{k,l} = h_{k,l}^* \quad , l = 1, ..., L, \quad k = 1, ..., N_{FFT} \tag{4.8}$$

- Equal Gain Combining (EGC):

$$EGC: \quad g_{k,l} = \frac{h_{k,l}^*}{\left|h_{k,l}^*\right|} \quad , l = 1, ..., L, \quad k = 1, ..., N_{FFT} \tag{4.9}$$

- Zero Forcing Combining (ZFC):

$$ZFC: \quad g_{k,l} = \frac{h_{k,l}^*}{\sum_{l=1}^{L} \left|h_{k,l}^*\right|^2} \quad , l = 1, ..., L, \quad k = 1, ..., N_{FFT} \tag{4.10}$$

- Minimum Mean Square Error Combining (MMSEC):

$$MMSEC: \quad g_{k,l} = \frac{h_{k,l}^*}{(\sum_{l=1}^{L} \left|h_{k,l}^*\right|^2 + \sigma^2)} \quad , l = 1, ..., L, \quad k = 1, ..., N_{FFT} \tag{4.11}$$

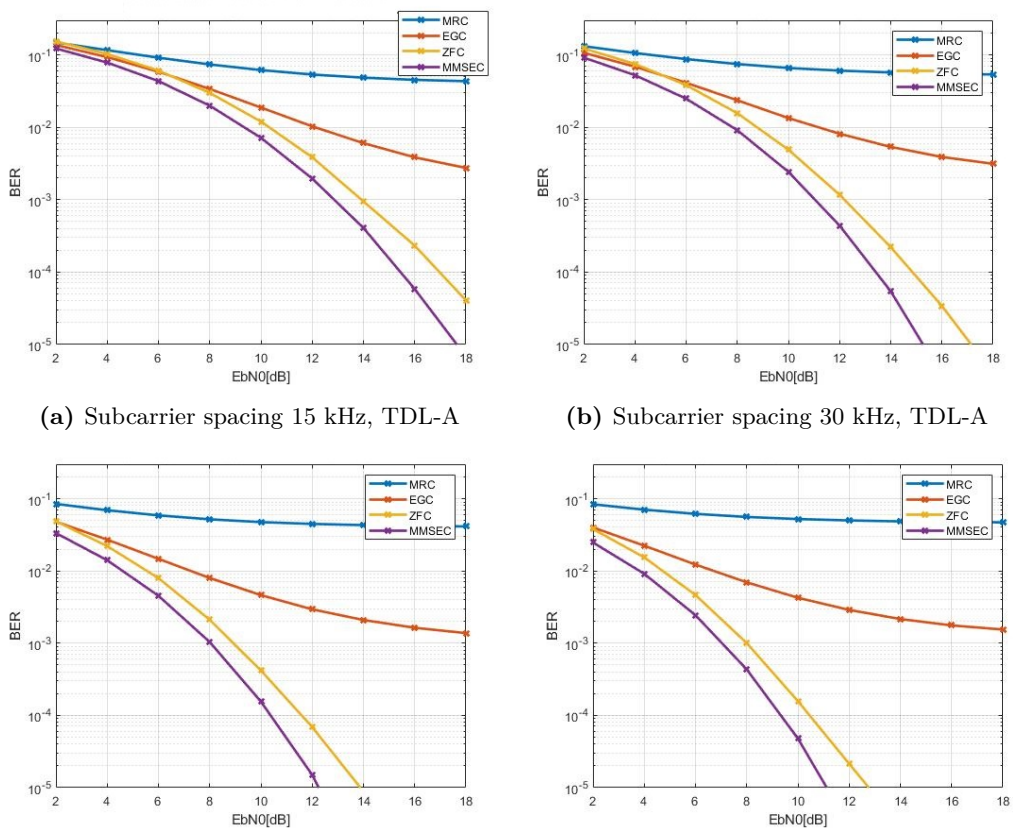

(a) Subcarrier spacing 15 kHz, TDL-A

(b) Subcarrier spacing 30 kHz, TDL-A

(c) Subcarrier spacing 60 kHz, TDL-A

(d) Subcarrier spacing 120 kHz, TDL-A

Figure 4.10: BER performance of DFT-s-OFDM equalizers on SIMO configuration

In this section we assume the same parameters presented in 4.1. The Figure 4.10 shows the performance results of the SIMO approach for $L = 2$ antennas for a DFT-s-OFDM system, using MRC, EGC, ZFC and MMSEC equalizers. We can observe that the SISO and SIMO case have a similar behavior and MMSEC outperforms the MRC, EGC, ZFC equalizers as well. As mentioned earlier the MMSEC can eliminate the ISI more efficiently. However, that behaviour is visible for lower values E_b/N_0. Looking to the Figure 4.7a and Figure 4.10a, SISO and SIMO scheme respectively, and having the MMSEC equalizer as reference with subcarrier spacing of 15 kHz, for a BER target of $1.0e^{-3}$, we obtained a performance improvement of approximately 7dB. Another important aspect to take from the Figure 4.10, is that ZFC and MMMSEC have approximately the same performance for SIMO scenario. In fact, the only advantage of MMSE over ZF is that it does not amplify too much the noise being able to cancel the ISI in a more efficient way. The improvement of EGC and MRC is very low because the orthogonality between subcarriers is destroyed by the interference, not being able then to take advantage of the spatial diversity introduced in the system. Hence, it is possible to conclude that multiple antennas systems, which introduces antenna and diversity gain, decreases the transmission errors and consequently increases the system performance.

The Figure 4.11 represents the results obtained for the scenario where we have the same

carrier separation but changing only the channels models used TDL-A, B and C. Similar to the situation in the SISO scheme, the performance of the system improves because of the frequency diversity order increases, as explained. Comparing again the results for various scheme of antennas, SISO and SIMO, the increased spatial diversity cleary improves the performance of the system. For instance, from SISO to SIMO case, for the TDL-B channel, we obtained a gain of approximately 7 dB for a BER target of 10^{-3}.

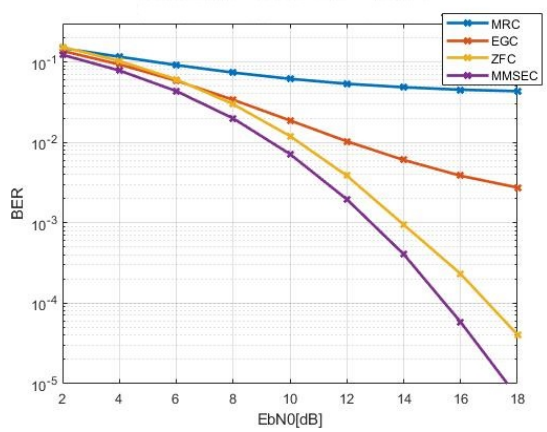

(a) Subcarrier spacing 15 kHz, TDL-A

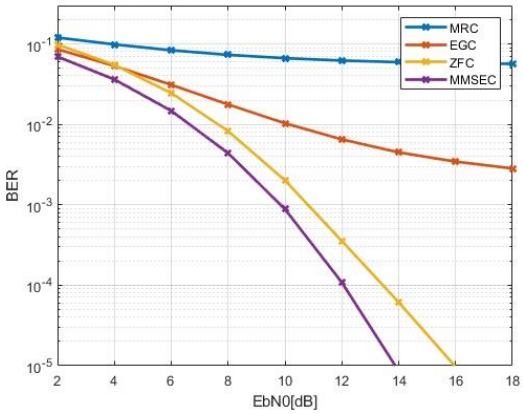

(b) Subcarrier spacing 15 kHz, TDL-B

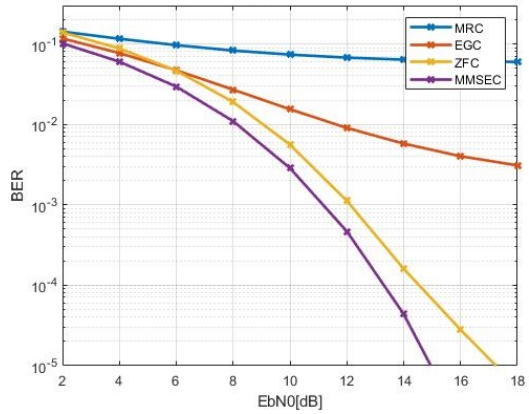

(c) Subcarrier spacing 15 kHz, TDL-C

Figure 4.11: BER performance for different TDL channels profiles with subcarrier separation 15 KHz

CHAPTER 5

Implemented iterative frequency-domain equalizer for 5G NR

To reach this goals like high bit rates, needed to meet the quality of service requirements of future multimedia applications, as mentioned, 5G NR has the capacity to support various numerologies and waveforms at UL. Comparing the performance of CP-OFDM and DFT-s-OFDM at the UL its possible to conclude that CP-OFDM based UL access can achieve better performance than DFT-s-OFDM signal [45]. However, its possible to improve the performance of a DFT-s-OFDM system with non linear techniques. This is possible because, despite the reasonable complexity/performance commitment obtained with linear equalizers schemes (see Chapter 4), they still have to deal with several problems inherent to its own nature, namely noise enhancement and residual ISI.

So, to improve the performance, non linear schemes such as decision feedback equalizers (DFEs) can be used instead, with one of the most promising being the IB-DFE, providing a good trade-off between complexity and performance. Contrarily to linear equalizers, it is composed by a feedforward and feedback filters implemented in the frequency domain that have the capacity of minimizing the impact of channel noise and ISI [46]. Therefore in this chapter we present the evaluation of the implemented iterative frequency-domain equalizers for DFT-s-OFDM. The chapter is organized into two main parts : single-user iterative equalizers, where we start by the SISO case and then we extend it for the case where the receiver is equipped with multiple antennas; and multi-user iterative equalizers, where a set of users transmit in the same time/frequency radio resources. Both approaches are evaluated for different 5G channel models and numerologies.

5.1 Single-user scenario

This section focuses on the principal aspects related with iterative frequency equalization implementation for the single-user case discussed in the Chapter 4. So a IB-DFE is presented and a structured process is adapted to the single-user DFT-s-OFDM. Two antennas configuration are considered: one where the base station is equipped only with one antenna SISO, another where the receiver are equipped with two antennas Single-Input Multiple-Output (SIMO) in order to exploit the advantages of spatial diversity. The equalization technique used in this single-user scenario was the MMSEC because of its lower noise enhancement effects. For the sake of comparison, both antennas scenarios, with non linear equalization, are going to be evaluated for different 5G numerologies and channels.

5.1.1 SISO Iterative Equalizer

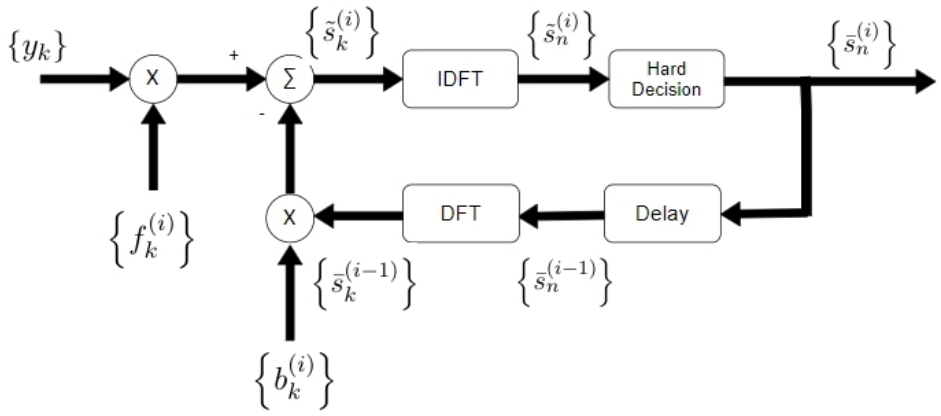

Figure 5.1: Siso IB-DFE receiver structure

The SISO iterative equalizer is presented in Figure 5.1. As can be seen, the received signal is firstly equalized in frequency domain by the feedforward filter f_k, followed by the IDFT and demodulation operations to obtain the first data estimates. Then the estimates are again converted to the frequency domain and multiplied by the feedback filter b_k and subtracted to the equalized received signal to remove the residual interference. This process is iteratively repeated until the data be successfully estimated, i.e. without interference. Still in the Figure 5.1, the index k and n associated to the ith iteration, represents that we are on the frequency and time domain, respectively.

The received signal y_k in the frequency domain, on a subcarrier k is given by:

$$y_k = h_k s_k + n_k \tag{5.1}$$

where h_k, s_k and n_k represents the transmit data, the subchannel and noise of the k^{th} subcarrier. To mitigate our channel effects we can apply a linear FDE, however the performance is much better if we replace a linear FDE by a IB-DFE, represented on figure 5.1. For a given iteration i^{th} the signal received in frequency-domain at the output of the equalizer is

$\left\{\tilde{s}_k^{(i)} : k = 0, 1, ...N_{DFT} - 1\right\}$ and can be written as [47],

$$\tilde{s}_k^i = f_k^{(i)} y_k - b_k^{(i)} \bar{s}_k^{(i-1)} \tag{5.2}$$

where $\left\{f_k^{(i)}; k = 0, 1, ..., N_{DFT} - 1\right\}$ is the feedforward coefficient and $\left\{b_k^{(i)}; k = 0, 1, ..., N_{DFT} - 1\right\}$ is the feedback coefficient . The $\left\{\bar{s}_k^{(i-1)}; k = 0, 1, ..., N_{DFT} - 1\right\}$ is kth DFT sample of the estimated block $\left\{\bar{s}_k^{(i-1)}; k = 0, 1, ..., N_{DFT} - 1\right\}$ from the previous iteration after the hard decision.

The feedforward and feedback coefficients, that defines the state of the detector at a give iteration, were chosen according the MMSEC, in order to maximize the Signal to Interference plus Noise Ratio (SINR), are given by

$$f_k^{(i)} = \frac{k_F^{(i)} h_k^*}{SNR + (1 - (p^{(i-1)})^2) |h_k|^2} \tag{5.3}$$

and

$$b_k^{(i)} = p^{(i-1)} (f_k^{(i)} h_k - 1) \tag{5.4}$$

respectively, where

$$SNR = \frac{E\left[|n_k|^2\right]}{E\left[|s_k|^2\right]} = \frac{1}{\sigma^2} \tag{5.5}$$

being,

$$\sigma^2 = \frac{\sigma_s^2}{\sigma_n^2} \tag{5.6}$$

with σ_n^2 denoting the variance of the noise term and σ_s^2 denoting the variance of the data symbols.

The correlation coefficient p, which can be regarded as the blockwise reliability of the decisions used in the feedback loop (from the previous iteration), is given by,

$$p^{(i-1)} = \frac{E\left[\bar{s}_n^{(i-1)} s_n^*\right]}{E\left[\left|s_n^{(*)}\right|^2\right]} \tag{5.7}$$

In order to normalize the signal received, k_F is selected so as to ensure that

$$\frac{1}{N_{DFT}} \sum_{k=0}^{N_{DFT}-1} f_k^{(i)} h_k = 1 \tag{5.8}$$

Looking closely to equation 5.3 , on the first iteration (i=0) , no information exists about s_k and the correlation coefficient in equation 5.7 is 0, what means that b_k is zero, as well . In this case the iterative equalizer reduces to the linear MMSEC given by 4.5. After the first iteration, the correlation factor tends to be $p \approx 1$, what means that, we have an almost full cancellation of the residual interference, being the result obtained approximate to the match filter [48].

5.1.2 IB-DFE with L-branch space diversity

In this section we extend the previous iterative equalizer designed for single antenna to multi-antennas case Figure 5.2, i.e., we assume that the base station is equipped with an antenna array with L antennas. The advantage of SIMO over SISO, is that extending the SISO IB-DFE receiver (Figure.5.1) to L antennas, the space diversity is going to improve, given then better BER results.

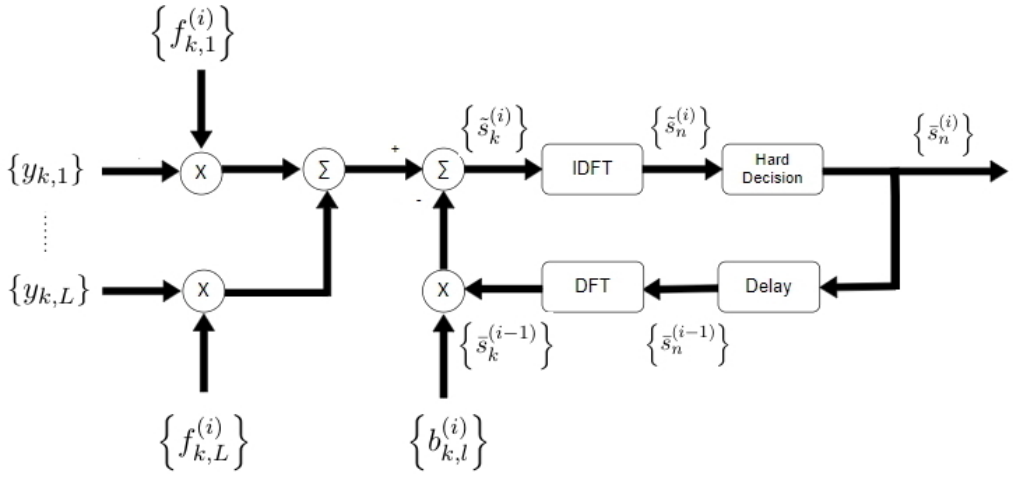

Figure 5.2: IB-DFE receiver with L-branch space diversity structure

Assuming that we have L receiver antennas, the received signal on time frequency after the multipath channel is characterized by,

$$y_{k,l} = h_{k,l}s_k + n_{k,l} \tag{5.9}$$

where $h_{k,l}$ and $n_{k,l}$ is the channel transfer function and the channel noise, respectively for the kth subchannel of the lth diversity branch [49].

Equally to the SISO IB-DFE we are going to have the $f_{k,l}$ and $b_{k,l}$, that are, respectively, the FeedForward an FeedBack coefficients matrix corresponding tho the ith iteration. At the output of the FDE the samples $\tilde{s}_k^{(i)}$ for the ith iteration are obtain as,

$$\tilde{s}_k^{(i)} = \sum_{l=1}^{L} f_{k,l}^{(i)} y_{k,l} - b_{k,l}^{(i)} \bar{s}_k^{(i-1)} \tag{5.10}$$

$\left\{\bar{s}_k^{(i-1)}; k = 0, 1, ..., N_{DFT} - 1\right\}$, represents the DFT block of hard decisions $\left\{\bar{s}_n^{(i-1)}; n = 0, 1, ..., N_{DFT} - 1\right\}$, of the iteration ($i$-1), associated to the block transmitted in the time domain $\{s_n; n = 0, 1, ..., N_{DFT} - 1\}$.

The feedforward coefficients, associated to the lth receive antenna is $\left\{f_{k,l}^{(i)}; k = 0, 1, ..., N_{DFT} - 1\right\}$ $(l = 1, 2, ..., L)$ and feedback coefficients are $\left\{b_{k,l}^{(i)}; k = 0, 1, ..., N_{DFT} - 1\right\}$ $(l = 1, 2, ..., L)$. Both are selected in order to optimize the SINR value.

The optimum feedback coefficients are given by

$$f_{k,l}^{(i)} = \frac{k_F^{(i)} * h_{k,l}^*}{SNR + (1 - (p^{(i-1)})^2) \sum_{l=1}^{L} |h_{k,l}|^2} \quad l = 1, 2, ..., L, \tag{5.11}$$

and

$$b_{k,l}^{(i)} = p^{(i-1)} (\sum_{l=1}^{L} f_{k,l}^{(i)} h_{k,l} - 1) \tag{5.12}$$

where $k_F^{(i)}$ is chosen in order to ensure we have normalised equalizers $\gamma^{(i)} = 1$, so we have [49],

$$\gamma^{(i)} = \frac{1}{N_{DFT}} \sum_{k=0}^{N_{DFT}-1} \sum_{l=1}^{L} f_{k,l}^{(i)} h_{k,l} \tag{5.13}$$

and the correlation factor $p^{(i-1)}$ is defined by the expression 5.7 and SNR is given by ,

$$SNR = \frac{E\left[|n_{k,l}|^2\right]}{E\left[|s_{k,l}|^2\right]} \tag{5.14}$$

Since the IB-DFE coefficients take into account the totality of the reliability block, the propagation error problem is significantly reduced. In general, IB-DFE techniques offer much better results promising than non-iterative methods. In fact, IB-DFE schemes can be considered as low-complexity turbo equalizers, because the feedback loop uses the equalizer outputs instead of the channel decoder outputs [50].

Like the SISO IB-DFE configuration, for the 1st interaction ($i = 0$) our optimum feedback coefficients, in the frequency-domain, are the same as the MMSE criterion presented in Eq.4.11. After some iterations, the correlation coefficient tends to be $p \approx 1$ and the residual ISI will be almost totally canceled, as well.

5.1.3 Numerical results

In this subsection, it is presented the performance results for both developed receiver structures. The results are presented in terms of average BER as a function of average bit energy per one-sided noise power spectral density ($\frac{E_b}{N_0}$). The key parameters used in this simulations was the same presented on Table 4.1. Both approaches are evaluated for different 5G channel models and numerologies.

The Figure 5.3 shows the results for TDL-A channel under various 5G numerologies presented in the tab 4.1. The results are also presented for 1 to 4 iterations. Focusing in the results, the first thing to conclude is that for the first iteration, as expected, the BER performance have the same behaviour as the standard linear MMSE equalization (Eq.4.5). As we can verify, when the number of iterations increases, the iterative interference cancellation works in a effective way, in witch by the time of the 4th iteration the performance tends to MFB performance. As we can see as well, the results obtained for iteration 3 are very close to the ones obtained to iteration 4. This means that 4 iteration are enough to remove most of the interference. Comparing then the linear SISO equalizer with the non-linear SISO, it is possible to see, for the better case scenario, that there is a improvement, with a BER of 10^{-5},

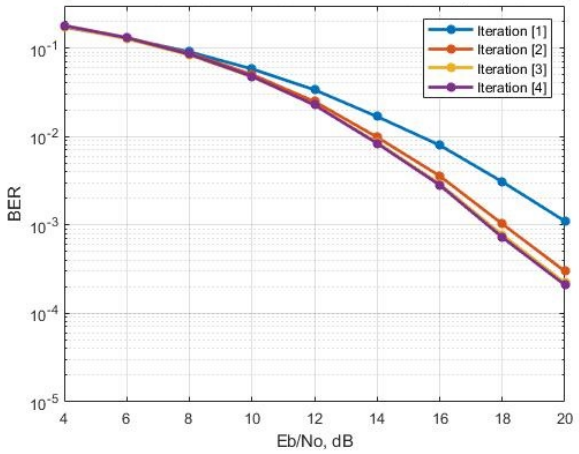

(a) Subcarrier spacing 15 kHz, TDL-A

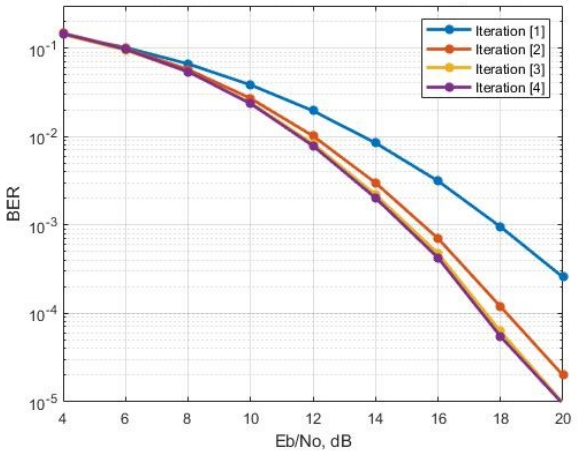

(b) Subcarrier spacing 30 kHz, TDL-A

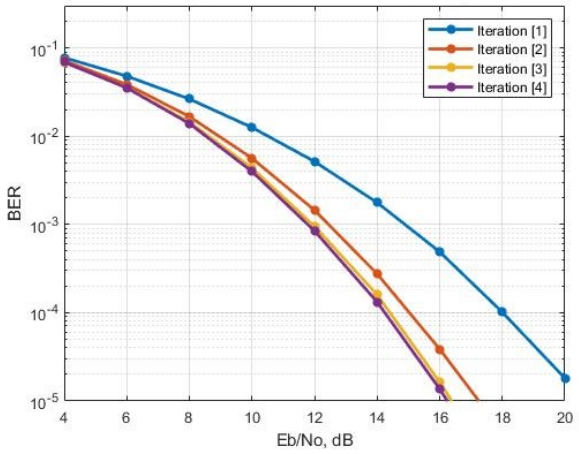

(c) Subcarrier spacing 60 kHz, TDL-A

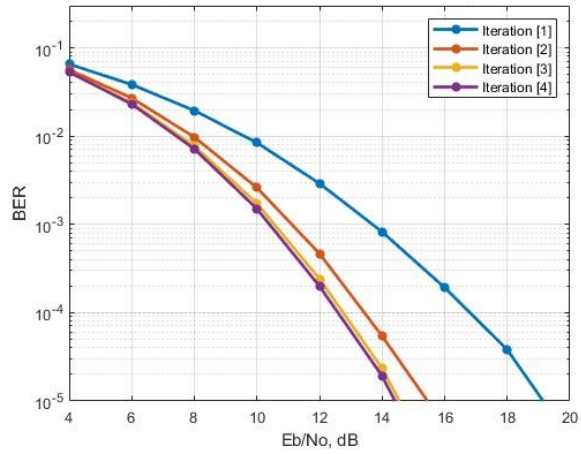

(d) Subcarrier spacing 120 kHz, TDL-A

Figure 5.3: BER performance for an IB-DFE receiver on SISO configuration

the difference is almost 3dB. Looking now for the results obtained for the different subcarrier separation, as mentioned earlier, we can see that our single-user system is going to present better results. With the increasing of the subcarrier separation the bandwidth is going to increase as well, what leads to the improvement of our inherent diversity order, improving then the BER result. For a BER of 10^{-3}, the difference between the case where we have a subcarrier separation of 120 kHz and 15 kHz is approximately 7dB.

The Figure 5.4 represents the results for the case where we have the same carrier separation of 15kHz but the channel model used is different. We can observe that with the increase of the delay spread the channel becomes more frequency selectivity improving then the performance system. The improvement between TDL-B and A is noticeable unlike B and C the results are almost the same.

The Figure 5.5 represents the case where the received is equipped with multiple antennas. As expected with the improving of the spatial diversity, we are going to obtain better performance results for the BER. It is possible to draw the same conclusions as for the results

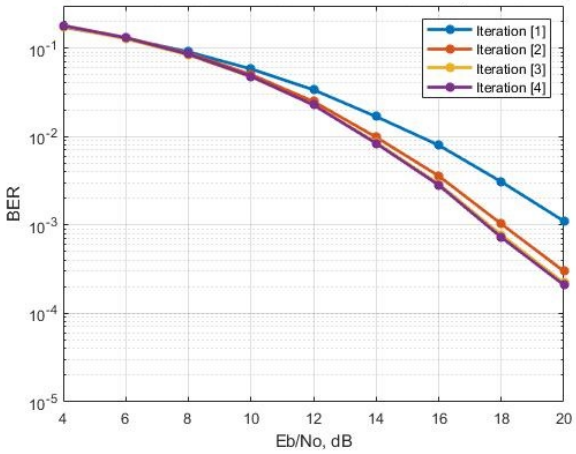

(a) Subcarrier spacing 15 kHz, TDL-A

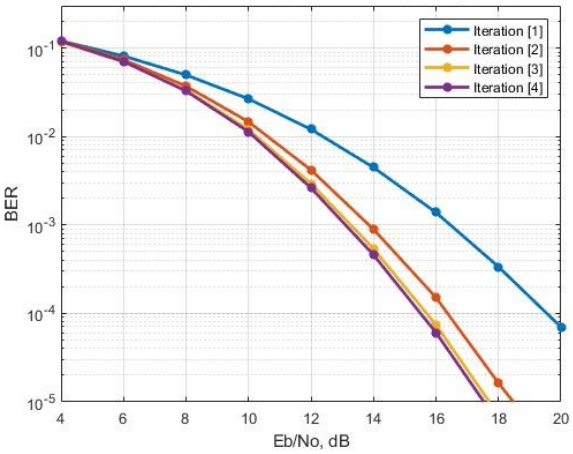

(b) Subcarrier spacing 15 kHz, TDL-B

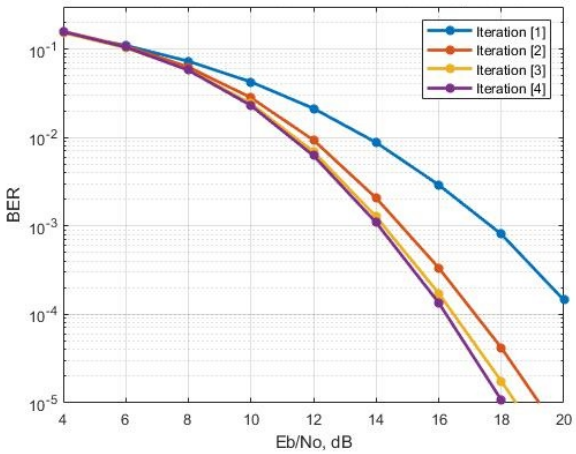

(c) Subcarrier spacing 15 kHz, TDL-C

Figure 5.4: BER performance for different TDL channels profiles with subcarrier separation 15 kHz

obtained for the linear equalizers. The gain obtained for a subcarrier separation of 15 kHz and for a BER of 10^{-3}, between SIMO and SISO scheme, is almost 6 dB, tendency which also applies for the other subcarrier separation.

About the impact of the TDL profile channels on BER performance in SIMO approach , (see Figure 5.6), the justification is the same as the SISO approach. Adding space diversity (jointly with inherent frequency diversity) to the system the overall performance improves as it can be seen in the presented results.

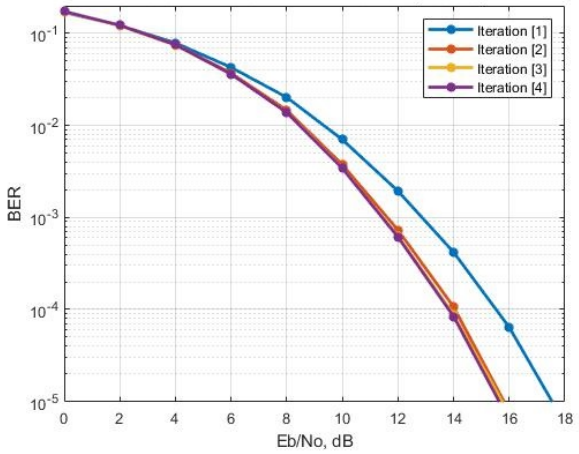

(a) Subcarrier spacing 15 kHz, TDL-A

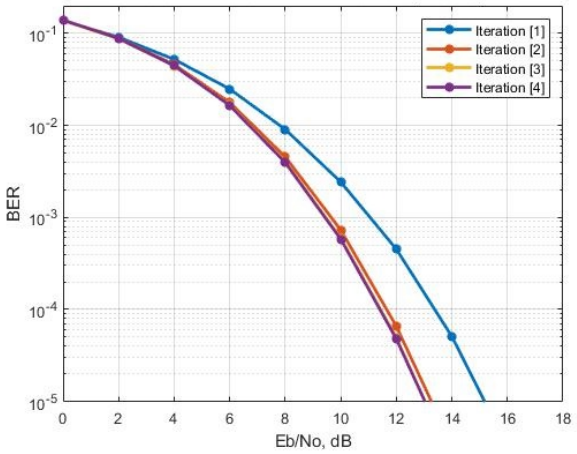

(b) Subcarrier spacing 30 kHz, TDL-A

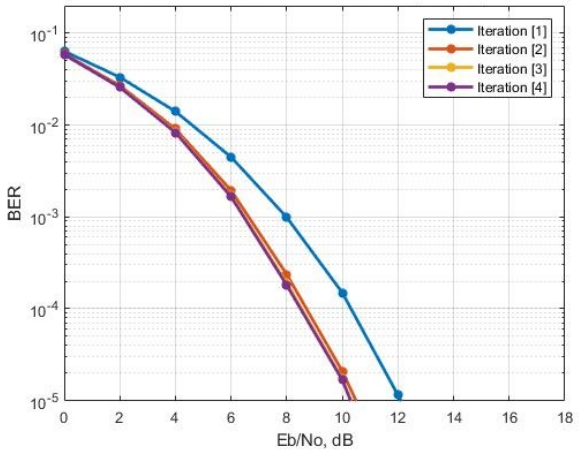

(c) Subcarrier spacing 60 kHz, TDL-A

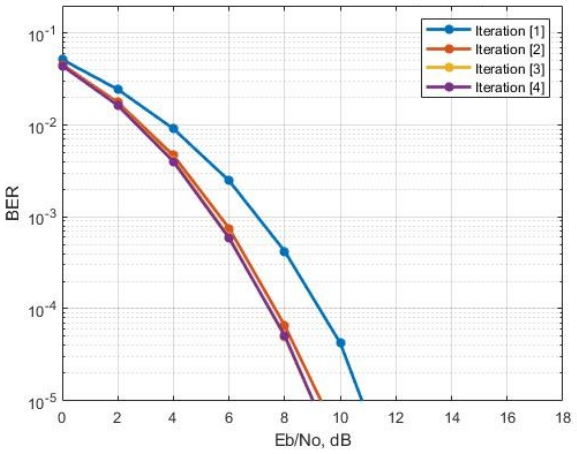

(d) Subcarrier spacing 120 kHz, TDL-A

Figure 5.5: BER performance for an IB-DFE receiver on SIMO configuration

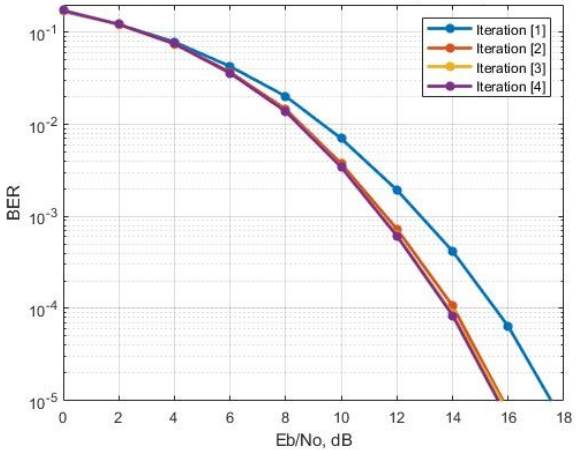

(a) Subcarrier spacing 15 kHz, TDL-A

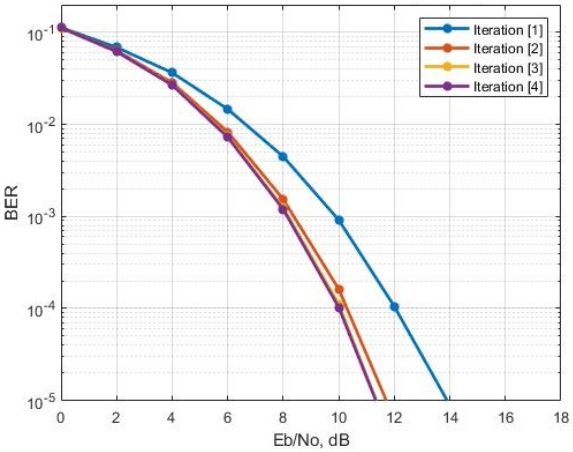

(b) Subcarrier spacing 15 kHz, TDL-B

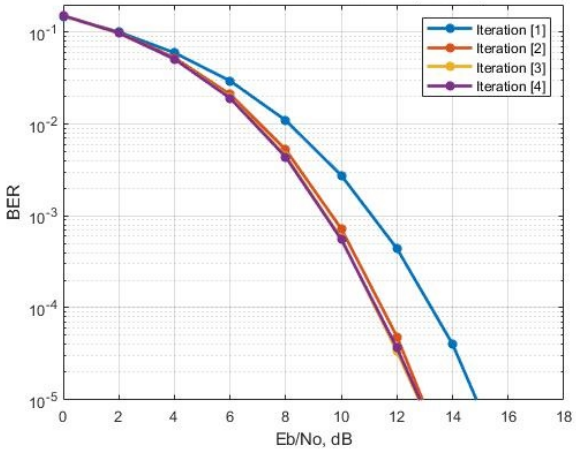

(c) Subcarrier spacing 15 kHz, TDL-C

Figure 5.6: BER performance for different TDL channels profiles with subcarrier separation 15 kHz

5.2 Multi-user scenario

MIMO techniques have gathered much attention in recent years as a way to improve drastically the performance of wireless mobile communications. This happens because in last decade, the number of mobile users have been significantly increased, tendency that will continue with 5G NR. A MIMO system can provide two types of gain: spatial diversity gain and spatial multiplexing gain [51]. In this scenario several users are allocated in the same set of carries having the equalizer to deal with both ISI and multi-user interference. So IB-DFE based equalizers has to deal with inter-user interference along with the ISI. In order to boost the data rate and fullfill the necessities of a 5G network its necessary to do extra processing like a subcarrier block sharing more than one user, as mentioned above. Finally, the implemented multi-user equalizer are detailed evaluated under several channel models and for different numerologies defined in the 5G NR.

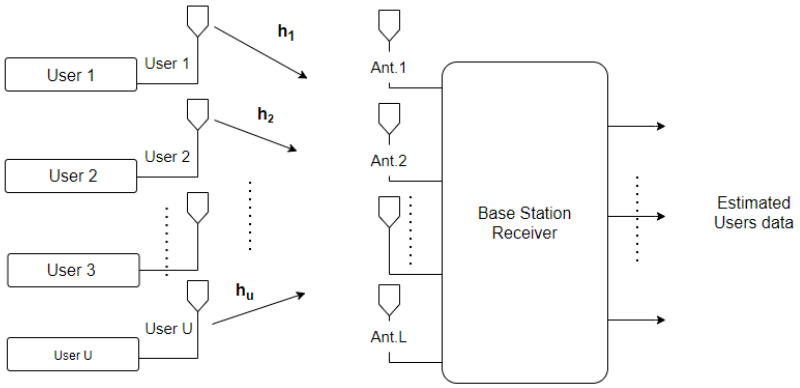

(a) MIMO configuration

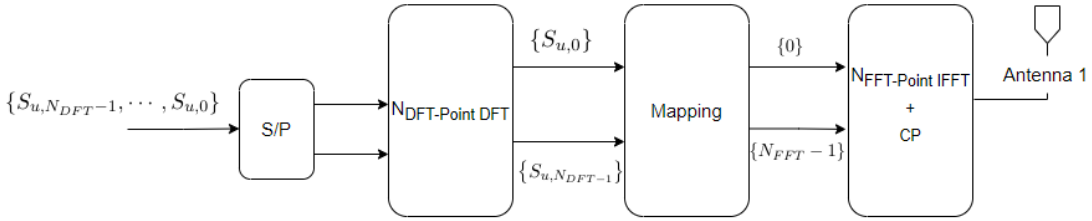

(b) DFT-S-OFDM transmitter for a generic user u

Figure 5.7: Multi-user System Characterization

The Figure 5.7a represents the MIMO configuration used in this section. As we can see in the Figure 5.7a we consider a base station equipped with L antennas and U with several single antenna transmitters sharing the same radio resources, i.e., same time slot and frequency band. In the Figure 5.7b, each user U sends data blocks, where the block associated to uth user $(u = 1, ..., U)$ in the frequency domain has the form $\{S_{u,k}; n = 0, ..., N_{DFT} - 1\}$, where k represents each subcarrier. The U users are going to be mapped on a same set of N_{DFT} length data block. After that, the frequency domain signals are interleaved so that they are widely separated in the OFDM symbol, therefore increasing the frequency diversity order.

5.2.1 Multi-user iterative MIMO Equalizer

The figure 5.8, represents the multi-user nonlinear equalizer implemented, where the feedforward and feedback operations are implemented in the frequency domain. In this system, all U users on kth subcarrier are detected, in a parallel way, improving then the estimation of transmitted data symbols. Updating the transmitted data with iterative processing is a promising way to filter out the effect of interferences, because for each iteration, the receiver's detection and adaptation of the feedforward and feedback equalizer coefficients minimizes the Mean Squared Error (MSE) at each subcarrier of the previous soft decisions [52].

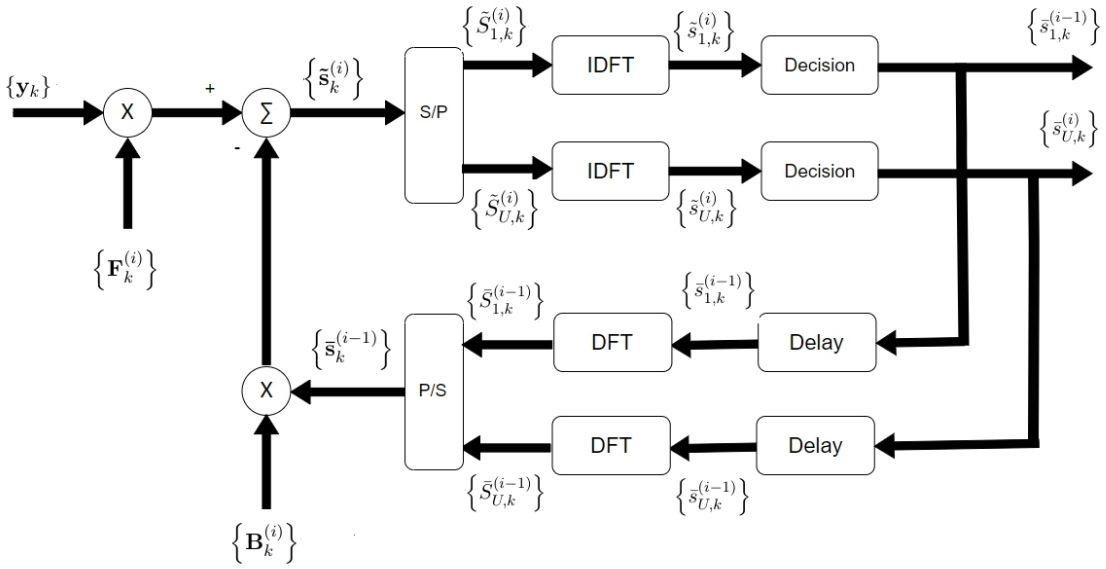

Figure 5.8: IB-DFE receiver structure PIC approach

At the receiver, after CP removal, N_{FFt}-point FFT operation, the received signal in frequency domain at the uth antenna and on kth subcarrier can be expressed in matrix format as

$$\mathbf{y}_k = \mathbf{H}_k^T \mathbf{s}_k + \mathbf{n}_k \tag{5.15}$$

with $\mathbf{y}_k = [y_{l,1}, ..., y_{L,k}]^T$, $\mathbf{n}_k = [y_{l,1}, ..., y_{L,k}]^T$, $\mathbf{s}_k = [s_{1,l}, ..., s_{l,k}]^T$, and

$$\mathbf{H}_k^T = \begin{bmatrix} h_{1,k}^{(1)} & \cdots & h_{U,k}^{(1)} \\ \vdots & \ddots & \vdots \\ h_{1,k}^{(L)} & \cdots & h_{U,k}^{(L)} \end{bmatrix} \tag{5.16}$$

The matrix $\mathbf{H}_k^T$ represents the frequency response of the channel between users and the receiver on subcarrier kth. The channel vector of the uth user is defined by, $\mathbf{h}_{u,k} = \left[h_{u,k}^{(1)}, ..., h_{u,k}^{(L)}\right]$.

Watching (Figure 5.8), for the ith iteration, the signal received, at the output of the equalizer, associated to kth subcarrier, is expressed by:

$$\tilde{\mathbf{s}}_k^{(i)} = \mathbf{F}_k^{(i)T}\mathbf{y}_k - \mathbf{B}_k^{(i)T}\bar{\mathbf{s}}_k^{(i-1)} \tag{5.17}$$

where $\mathbf{F}_k^{(i)} = \left[\mathbf{f}_{1,k}^{(i)}, ..., \mathbf{f}_{U,k}^{(i)}\right]$ is a matrix of size UxL with all u users feedforward vector coefficients, $\mathbf{B}_k^{(i)} = \left[\mathbf{b}_{1,k}^{(i)}, ..., \mathbf{b}_{U,k}^{(i)}\right]^T$ denoting the feedback vector coefficients of size UxU with all users and $\tilde{\mathbf{s}}_n^{(i)} = \left[s_{1,k}^{(i)}, ..., s_{U,k}^{(i)}\right]^T$.

The feedforward and feedback matrices are computed by minimizing the MSE between the estimated symbols and the transmitted symbols at the detection point of the receiver. For a QSPK constellation, the average BER can be approximately given by

$$BER \approx Q\left(\sqrt{(\frac{K}{\frac{1}{N_{DFT}}\sum_{k=0}^{N_{DFT}-1} MSE_n})}\right) \tag{5.18}$$

The MSE_k can be formulated as,

$$\begin{aligned} MSE_k = tr(\mathbf{F}_k^H\mathbf{R}_k^{\mathbf{Y}}\mathbf{F}_k) + tr(\mathbf{B}_k^H\mathbf{R}^{\bar{\mathbf{S}},\bar{\mathbf{S}}}\mathbf{B}_k) + K\sigma_s^2 - 2tr(Re\left\{\mathbf{F}_k^H\mathbf{R}_k^{\mathbf{Y},\mathbf{S}}\right\}) + \\ 2tr(Re\left\{\mathbf{B}_k^H\mathbf{R}^{\bar{\mathbf{S}},\mathbf{S}}\right\}) + -2tr(Re\left\{\mathbf{B}_k^H\mathbf{R}_k^{\bar{\mathbf{S}},\mathbf{Y}}\mathbf{F}_k\right\}) \end{aligned} \tag{5.19}$$

with the correlation matrices defined as,

$$\begin{cases} \mathbf{R}_k^{\mathbf{Y}} = \mathbb{E}\left[\mathbf{Y}_k^*\mathbf{Y}_k^T\right] = \mathbf{H}_k^H\mathbf{R}_S\mathbf{H}_k + \mathbf{R}_{N_{DFT}} \\ \mathbf{R}^{\bar{\mathbf{S}},\bar{\mathbf{S}}} = \mathbb{E}\left[\bar{\mathbf{S}}^*\bar{\mathbf{S}}^T\right] = \mathbf{P}^2\mathbf{R}_S \\ \mathbf{R}_k^{\mathbf{Y},\mathbf{S}} = \mathbb{E}\left[\mathbf{Y}^*\mathbf{S}_k\right] = \mathbf{H}_k^H\mathbf{R}_S \\ \mathbf{R}^{\bar{\mathbf{S}},\mathbf{S}} = \mathbb{E}\left[\bar{\mathbf{S}}^*\mathbf{S}_k\right] = \mathbf{H}_k^H\mathbf{R}_S \\ \mathbf{R}_k^{\bar{\mathbf{S}},\mathbf{Y}} = \mathbb{E}\left[\bar{\mathbf{S}}^*\mathbf{Y}_k\right] = \mathbf{P}^2\mathbf{R}_S\mathbf{H}_k \end{cases}$$

The optimization problem to compute the feedforward and feedback can be formulated as [53],

$$minMSE_k \quad s.t \quad \frac{1}{N_{DFT}}\sum_{k=0}^{N_{DFT}} tr(\mathbf{F}_k^T\mathbf{H}_k^T) = U \tag{5.20}$$

By employing the Lagrange multiplier's method, and after some straightforward but lengthy mathematical manipulations, we obtain the solution for both the feedforward and feedback matrices, given by [53]

$$\mathbf{F}_k^{(i)} = \left(\mathbf{H}_k^{(H)}(\mathbf{I}_U - \mathbf{P}^{(i-1)^2})\mathbf{H}_k + \frac{\sigma_N^2}{\sigma_S^2}\mathbf{I}_L\right)^{-1}\mathbf{H}_k^{(H)}\mathbf{\Omega}^i \tag{5.21}$$

and

$$\mathbf{B}_k^{(i)} = \mathbf{H}_k\mathbf{F}_k^{(i)} - \mathbf{I}_U \tag{5.22}$$

with,

$$\mathbf{\Omega}^{(i)} = (\mathbf{I}_U - \mathbf{P}^{(i-1)^2}) - \frac{\mu^{(i)}}{\sigma_S^2 N_{DFT}}\mathbf{I}_U \tag{5.23}$$

The correlation coefficients can be defined as $\mathbf{P} = diag(p_1 ..., p_U)$,

$$p_k = \frac{\mathbb{E}\left[\tilde{s}_{u,k} s_{u,k}^*\right]}{\mathbb{E}\left[|s_{u,k}|^2\right]} \tag{5.24}$$

In this type of system for the first iteration (i), no information exists about s_k which means the vector $\bar{\mathbf{s}}_\mathbf{k}^\mathbf{0}$ is null and $\mathbf{P}^{(0)}$ is a null matrix as well. This reduce the system to a conventional multi-user MMSE equalizer for the first iteration, but with the increase of the iterations the matrix $\mathbf{P}^{(i-1)}$ tends to an identity matrix, witch means that the multi-user and ISI interferences were successfully removed.

5.2.2 Performance results

In this section the performance results of the implemented multi-user iterative block frequency domain equalizer are presented and discussed. The key parameters used in the simulation are the same as the Table 4.1. The unique difference is that for this scenario our system is going to be equipped with multiple antennas. We assume $U = 4$ users transmitting in the same resources and a receiver equipped with L antennas. In the matters of channel model, its going to be used the TDL channel models already mentioned. The results are presented in form of a BER in function of $\frac{E_b}{N_0}$, similar to the single-user scenario 4 iterations is going to be made.

Looking now to the performance in Figure 5.9, we can see that the BER curve presents better results when compared with the other scenarios already evaluated. For a MIMO 4x4 scheme and having a BER reference of 10^{-3}, for the last iteration we have a $\frac{E_b}{N_0}$ approximately of 9 dB. It its noticeable to, a better improvement on the performance system between the iterations. In the MIMO mode between the 1^{st} and the 2^{st} we have a improvement of approximately 6 dB, while in the SIMO scenario for example we are going to have a improvement close to the 2dB. It can be observed that with only a four iterations almost all multi-user interference is removed.

The Figure 5.10 shows the impact of the various TDL channels on the multi-user system. As expected the behaviour of this results are going to be the same as the other scenarios (SISO and SIMO single-user system). The only difference is that for the MIMO scenario we are going to have higher order diversity in the system improving then the BER results. In a conclusion to this section we can say, because of the better BER results, that the MIMO multi-user scenario takes more advantage of the fact that we have higher space-diversity order available, meaning that this scenario is more efficient in removing both multi-user and inter-carrier interferences.

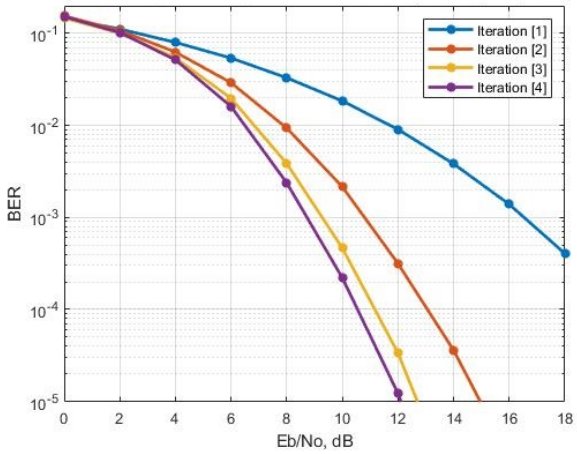

(a) Subcarrier spacing 15 kHz, TDL-A

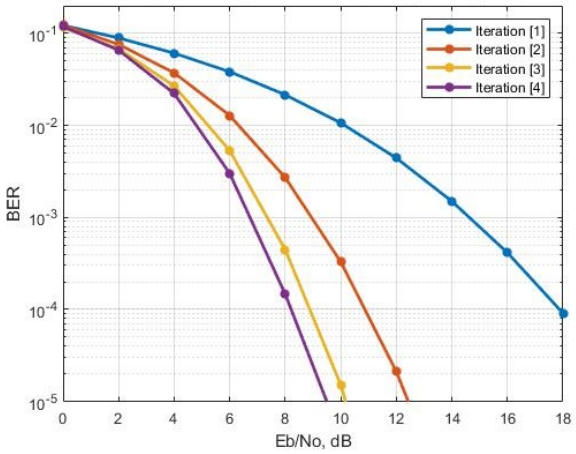

(b) Subcarrier spacing 30 kHz, TDL-A

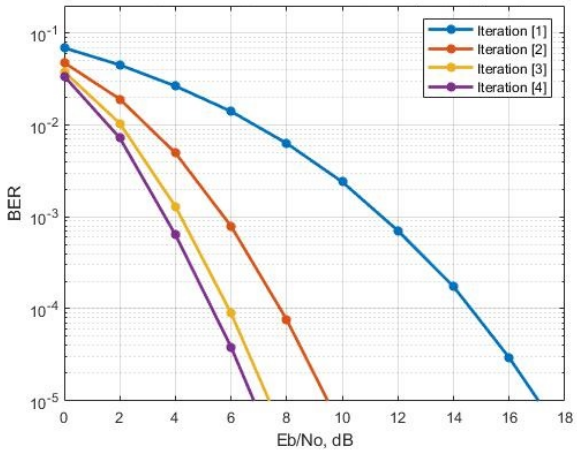

(c) Subcarrier spacing 60 kHz, TDL-A

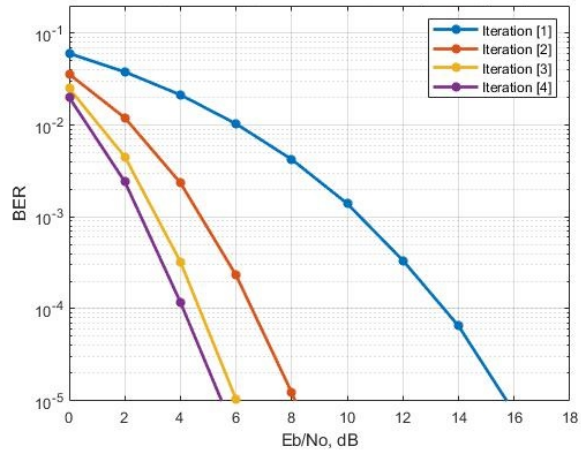

(d) Subcarrier spacing 120 kHz, TDL-A

Figure 5.9: BER performance for an IB-DFE receiver on PIC approach, MIMO 4x4 configuration

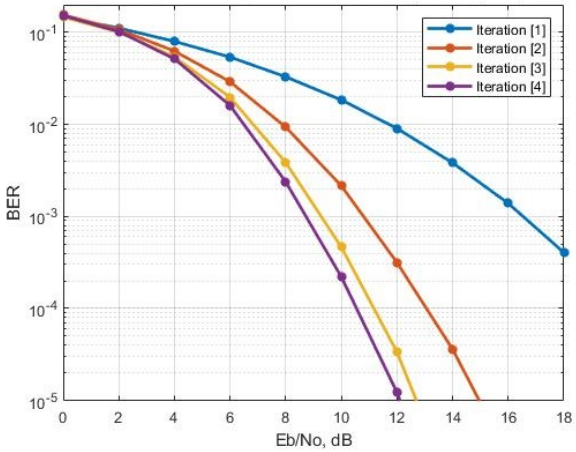

(a) Subcarrier spacing 15 kHz, TDL-A

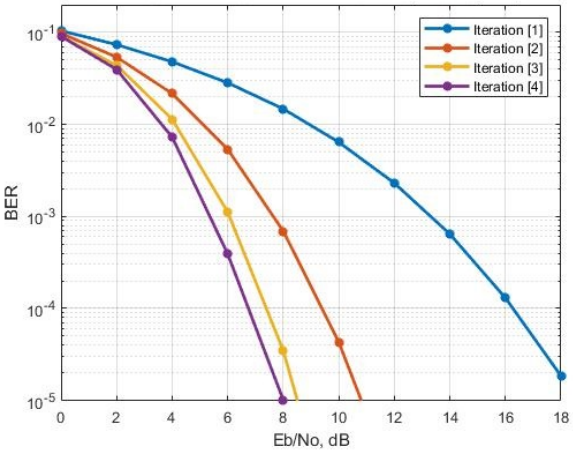

(b) Subcarrier spacing 15 kHz, TDL-B

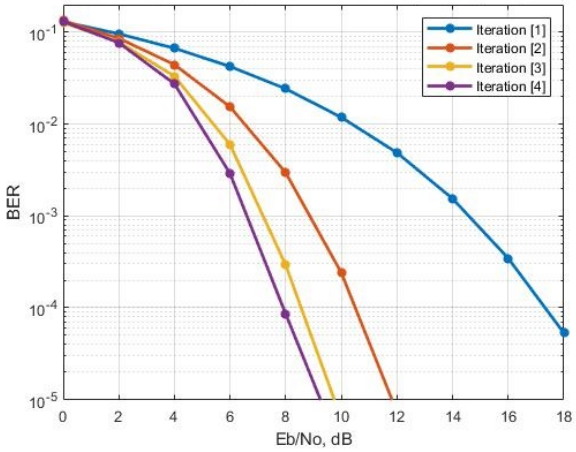

(c) Subcarrier spacing 15 kHz, TDL-C

Figure 5.10: BER performance for different TDL channels profiles with subcarrier separation 15 kHz

CHAPTER 6

Conclusions

This dissertation started by presenting the background and evolution of cellular communications systems, from the 1st to the 5th generation. Focusing first on multiple access techniques, such as the FDMA in 1G communication systems, the TDMA in 2G communication systems, the CDMA in 3G communication systems, and the OFDMA for 4G communication systems. Finally, the motivation that leads to the development of this thesis was presented.

In the Chapter 2 was provided a general overview of the 5G system. Giving details about the services and applications used in 5G, technical performance requirements, frequency spectrum and finally the different channel models discussed for 5G NR.

The Chapter 3 described the principal aspects of the physical layer supporting 5G, emphasizing the different numerologies proposed for 5G NR. The principal characteristics of each of these different numerologies was presented. This was important because the implemented single and multi-user were evaluated using the different numerologies proposed, in order to assess how its performance is affected.

The Chapter 4 introduced the principles of the transmission technique DFT-s-OFDM. Then, the linear equalization schemes were presented and evaluated for the different 5G numerologies. The analysis of results showed that the MMSEC equalizer presents better BER performance than ZFC, EGC and MRC. For scenarios with better spatial diversity, SIMO scenario, the ZFC presents a performance close to the MMSEC equalizer. The ZFC becomes relevant because it does not need to estimate the noise variance. In general the MRC equalizer is the one with the worst results in terms of BER. In relation to the impact of the various numerologies and channel models we can conclude that as the value, of the subcarrier spacing and delay spread of the TDL profile increases the performance of the proposed system improves as well. This is due to the higher frequency diversity order added to the system, leading to a performance improvement. Because of the low complexity of the linear equalizers, they still suffer from noise enhancement and residual ISI.

The chapter 5, we firstly presented the single-user receiver structure, for the uplink transmission of DFT-s-OFDM systems, based on non-linear techniques (IB-DFE) as an

alternative to the linear equalizers presented in Chapter 4. In this first approach two antennas configuration was considered, a SISO and SIMO. In this system for each user was assumed, that each one uses a different set of subcarriers so the non linear equalizer just needed to deal with ISI. Secondly, on the second scenario it was described a multi-user case, where the same set of carries were allocated to the several users in order to increase the data rate. In this case the equalizer dealt with both ISI and ICI. The transmitter and base station were equipped with U single antennas and L antennas, respectively. Therefore, the multi-user MIMO scheme is performed by various single user antenna that communicates with a multi-antenna Base Station. For both cases, several performance simulations were done, with the objective of evaluate the different numerologies and TDL channels defined in the 5G. The results are presented in terms of average BER as a function of average bit energy per one-sided noise power spectral density ($\frac{E_b}{N_0}$) and also presented for 1 to 4 iterations. The main conclusions to retain for each scenario, are:

- *Single-user:* In this scenario with the non linear equalizer, the result of the first iteration corresponds to a conventional linear MMSE equalizer and the subsequent iterations provides better results for BER, thanks to the iterative cancellation of residual interference. As mentioned before, with the improvement of the spatial diversity in our system (SIMO scheme), we are able to obtain better results for the BER.
- *Multi-user:* The multiple antenna systems allow exploiting diversity and spatial multiplexing, solutions to achieve high bit rates. The implemented receiver proposed mitigates the inter-user and ISI interference, improving the overall system results.

To sum up, it was showed that non linear equalizer IB-DFE shows better performances when comparing with linear equalizers, and about the impact of the different numerologies and TDL channels, with the increase of the subcarrier separation and delay spread of the TDL profile, the inherent frequency diversity of the system will improve. So the overall system performance will improve too , resulting in better results for the BER.

6.1 Future Work

Taking into account to work developed so far, there are a few ideas that could be further developed on future work,

- In this work, channel coding was not applied, turning interesting the channel coding considered in 5G NR in order to evaluate the performance of the implemented equalizers in a more realistic scenario.
- It was considered perfect channel information at the base station. In practical systems the channel is estimated with errors, therefore it would be interesting to evaluate the implemented solutions under imperfect channel state information.

References

[1] E. Dahlman, S. Parkvall, and J. Sköld, *5G NR: The Next generation wireless Access technology*, 2018. DOI: 10.1016/C20170013472. [Online]. Available: https://www.elsevier.com/books/5g-nr-the-next-generation-wireless-access-technology/dahlman/978-0-12-814323-0.

[2] I. Update, O. N. The, P. Of, and T. H. E. Networked, "Mobility Report," no. June, pp. 4–7, 2021. [Online]. Available: https://www.ericsson.com/49cd40/assets/local/mobility-report/documents/2021/june-2021-ericsson-mobility-report.pdf.

[3] J. N. Syed, S. K. Sharma, S. Wyne, M. Patwary, and M. Asaduzzaman, "Quantum machine learning for 6g communication networks: State-of-the-art and vision for the future," *IEEE Access*, vol. 7, pp. 46 317–46 350, Apr. 2019. DOI: 10.1109/ACCESS.2019.2909490.

[4] F. H. Blecher, *Advanced Mobile Phone Service*, 1980. DOI: 10.1109/T-VT.1980.23847. [Online]. Available: https://searchmobilecomputing.techtarget.com/definition/Advanced-Mobile-Phone-Service.

[5] U. Mitra, "Spread-Spectrum Systems," in *Encyclopedia of Physical Science and Technology*, Elsevier, Jan. 2003, pp. 667–694. DOI: 10.1016/b0-12-227410-5/00722-5.

[6] B. A. Kumar and P. T. Rao, "Overview of advances in communication technologies," *INCEMIC 2015 - 13th International Conference on Electromagnetic Interference and Compatibility, Proceedings*, pp. 102–106, 2017. DOI: 10.1109/INCEMIC.2015.8055856.

[7] E. Dahlman, S. Parkvall, and J. Sköld, "4g, LTE Evolution and the Road to 5G," in *4g, LTE Evolution and the Road to 5G*, Elsevier, Jan. 2016, pp. 1–5. DOI: 10.1016/b978-0-12-804575-6.00001-7.

[8] Qualcomm, "The Evolution of Mobile Technologies: 1G 2G 3G 4G LTE," Tech. Rep., 2014.

[9] H. Wymeersch and A. Eryilmaz, "Multiple access control in wireless networks," in *Academic Press Library in Mobile and Wireless Communications: Transmission Techniques for Digital Communications*, Elsevier, Jul. 2016, pp. 435–465, ISBN: 9780123972224. DOI: 10.1016/B978-0-12-398281-0.00012-0.

[10] B. Hjelm, "Standards and Intellectual Property Rights in the Age of Global Communication - A Review of the International Standardization of Third-Generation Mobile System," *arXiv*, vol. 3, no. October 1997, 2000.

[11] R. M. Buehrer, "Code Division Multiple Access(CDMA)," *Synthesis Lectures on Communications*, vol. 2, pp. 1–192, Jan. 2006, ISSN: 19321708. DOI: 10.2200/s00017ed1v01y200508com002.

[12] M. Hossain, M. Rahman, and A. Alim, "Performance Analysis of Uplink Downlink Transmission in CDMA System," *Journal of Telecommunications*, vol. 1, no. 1, pp. 84–86, 2010. [Online]. Available: http://sites.google.com/site/journaloftelecommunications/.

[13] 3GPP, *LTE*, 2008. [Online]. Available: https://www.3gpp.org/technologies/keywords-acronyms/98-lte.

[14] M. Rumney, *LTE and the Evolution to 4G Wireless: Design and Measurement Challenges: Second Edition*. Wiley Blackwell, Jul. 2013, pp. 1–626, ISBN: 9781118799475. DOI: 10.1002/9781118799475.

[15] B. Andre and V. Robson, "Orthogonal Frequency Division Multiple Access Fundamentals and Applications," *Orthogonal Frequency Division Multiple Access Fundamentals and Applications*, vol. Chapter 21, p. 30, Apr. 2010. DOI: 10.1201/9781420088250. [Online]. Available: https://www.researchgate.net/publication/235945562_Orthogonal_Frequency_Division_Multiple_Access_Fundamentals_and_Applications.

[16] S. P. Yadav and S. C. Bera, "Papr analysis of single carrier fdma system for uplink wireless transmission," in *2015 10th International Conference on Information, Communications and Signal Processing (ICICS)*, 2015, pp. 1–5. DOI: 10.1109/ICICS.2015.7459941.

[17] ETSI, "3GPP TS 36.101 version 14.3.0 Release 14," *European Telecommunications*, vol. 14, p. 1370, 2017. [Online]. Available: https://www.etsi.org/deliver/etsi_ts/136100_136199/136101/08.02.00_60/ts_136101v080200p.pdf.

[18] ITU-R, "IMT Vision – Framework and overall objectives of the future development of IMT for 2020 and beyond," *Itu-R M.2083-0*, no. September 2015, https://www.itu.int/dms$_p$*ubrec/itu* − −*r/rec/m/R* − −*REC˜M*, 2015. [Online]. Available: https://itu.int/dms_pubrec/itu-r/rec/m/R-REC-M.2083-0-201509-I!!PDF-E.pdf.

[19] A. Sahin, E. Bala, R. Yang, and R. L. Olesen, "DFT-Spread OFDM with Frequency Domain Reference Symbols," *2017 IEEE Global Communications Conference, GLOBECOM 2017 - Proceedings*, vol. 2018-January, pp. 1–6, Jul. 2017. DOI: 10.1109/GLOCOM.2017.8254241.

[20] D. Castanheira, A. Silva, R. Dinis, and A. Gameiro, "Efficient transmitter and receiver designs for sc-fdma based heterogeneous networks," *IEEE Transactions on Communications*, vol. 63, no. 7, pp. 2500–2510, 2015. DOI: 10.1109/TCOMM.2015.2434383.

[21] N. Benvenuto and S. Tomasin, "Iterative design and detection of a DFE in the frequency domain," *IEEE Transactions on Communications*, vol. 53, no. 11, pp. 1867–1875, Nov. 2005. DOI: 10.1109/TCOMM.2005.858666.

[22] R. Dinis, A. Gusmao, and N. Esteves, "On broadband block transmission over strongly frequency-selective fading channels," *IEEE Wireless 2003*, 2003.

[23] 3GPP, *Release 15*, 2018. [Online]. Available: https://www.3gpp.org/release-15.

[24] H. Atarashi, M. Iwamura, S. Nagata, T. Nakamura, and A. Toskala, "5g targets and standardization," in *5G Technology*. John Wiley Sons, Ltd, 2020, ch. 2, pp. 13–25, ISBN: 9781119236306. DOI: https://doi.org/10.1002/9781119236306.ch2. eprint: https://onlinelibrary.wiley.com/doi/pdf/10.1002/9781119236306.ch2. [Online]. Available: https://onlinelibrary.wiley.com/doi/abs/10.1002/9781119236306.ch2.

[25] S. E. Elayoubi, M. Fallgren, P. Spapis, G. Zimmermann, D. Martín-Sacristán, C. Yang, S. Jeux, P. Agyapong, L. Campoy, Y. Qi, and S. Singh, "5g service requirements and operational use cases: Analysis and metis ii vision," in *2016 European Conference on Networks and Communications (EuCNC)*, 2016, pp. 158–162. DOI: 10.1109/EuCNC.2016.7561024.

[26] E. Mohyeldin, "09 - Minimum Technical Performance Requirements for IMT-2020 radio interface(s)," pp. 1–12, 2016. [Online]. Available: https://www.itu.int/en/ITU-R/study-groups/rsg5/rwp5d/imt-2020/Documents/S01-1_Requirements%20for%20IMT-2020_Rev.pdf.

[27] RajJain, ""Channel Models: A Tutorial", WiMAX Forum AATG," *WiMAX Forum*, pp. 1–21, 2007. [Online]. Available: http://www.cse.wustl.edu/$%5Csim$jain/cse574-08/ftp/channel_model_tutorial.pdf.

[28] ETSI, "TS 138 104 - V15.3.0 - 5G; NR; Base Station (BS) radio transmission and reception (3GPP TS 38.104 version 15.3.0 Release 15)," vol. 0, p. 160, 2018. [Online]. Available: https://portal.etsi.org/TB/ETSIDeliverableStatus.aspx.

[29] *New Radio - NI*. [Online]. Available: https://www.ni.com/pt-pt/innovations/wireless/5g/new-radio.html (visited on 09/10/2021).

[30] N. Cvijetic, "OFDM for Next-Generation Optical Access Networks," *JOURNAL OF LIGHTWAVE TECHNOLOGY*, vol. 30, no. 4, 2012. DOI: 10.1109/JLT.2011.2166375. [Online]. Available: http://ieeexplore.ieee.org..

[31] H. Holma, A. Toskala, and T. Nakamura, *5G technology : 3GPP new radio*. 2020, vol. 148, pp. 61–62, ISBN: 9781119236313.

[32] M. Sandell, "Design and Analysis of Estimators for Multicarrier Modulation and Ultrasonic Imaging," 1996.

[33] Qualcomm, "Making 5G NR a reality :Leading the technology inventions for a unifi ed, more capable 5G air interface," no. December, 2016.

[34] ETSI, "5G NR Physical channels and modulation (3GPP TS 38.211 version 15.2.0 Release 15)," *Ts 138 211 - V15.2.0*, vol. 2, pp. 1–98, 2018.

[35] J. F. de Valgas, J. F. Monserrat, and H. Arslan, "Flexible numerology in 5G NR: Interference quantification and proper selection depending on the scenario," *Mobile Information Systems*, vol. 2021, 2021, ISSN: 1875905X. DOI: 10.1155/2021/6651326.

[36] C. Oberli and M. García, "Intercarrier interference in OFDM: A general model for transmissions in mobile environments with imperfect synchronization," *Eurasip Journal on Wireless Communications and Networking*, vol. 2009, no. 1, pp. 1–11, Nov. 2009, ISSN: 16871472. DOI: 10.1155/2009/786040. [Online]. Available: https://jwcn-eurasipjournals.springeropen.com/articles/10.1155/2009/786040.

[37] Y. S. Cho, J. Kim, W. Y. Yang, and C. G. Kang, "MIMO-OFDM Wireless Communications with MATLAB®," *MIMO-OFDM Wireless Communications with MATLAB®*, p. 457, 2010. DOI: 10.1002/9780470825631.

[38] S. Ahmadi, "5G NR: Architecture, technology, implementation, and operation of 3GPP new radio standards," *5G NR: Architecture, Technology, Implementation, and Operation of 3GPP New Radio Standards*, pp. 1–960, Jan. 2019. DOI: 10.1016/C2016-0-04944-6.

[39] TSGR, "TS 138 213 - V15.7.0 - 5G; NR; Physical layer procedures for control (3GPP TS 38.213 version 15.7.0 Release 15)," 2019. [Online]. Available: https://portal.etsi.org/TB/ETSIDeliverableStatus.aspx.

[40] S. Sirotkin, "5G Radio Access Network Architecture: The Dark Side of 5G," *5G Radio Access Network Architecture: The Dark Side of 5G*, 2021. DOI: 10.1002/9781119550921.

[41] A. F. Demir, M. H. Elkourdi, M. Ibrahim, and H. Arslan, "Waveform design for 5G and beyond," *5G Networks: Fundamental Requirements, Enabling Technologies, and Operations Management*, pp. 51–76, Jan. 2018. DOI: 10.1002/9781119333142.ch2. arXiv: 1902.05999. [Online]. Available: https://onlinelibrary.wiley.com/doi/full/10.1002/9781119333142.ch2%20https://onlinelibrary.wiley.com/doi/abs/10.1002/9781119333142.ch2%20https://onlinelibrary.wiley.com/doi/10.1002/9781119333142.ch2.

[42] A. Al-Dweik, A. Hazmi, B. Sharif, and C. Tsimenidis, "Efficient interleaving technique for OFDM system over impulsive noise channels," *IEEE International Symposium on Personal, Indoor and Mobile Radio Communications, PIMRC*, pp. 167–171, 2010. DOI: 10.1109/PIMRC.2010.5671925.

[43] A. Pereira, P. Bento, M. Gomes, R. Dinis, and V. Silva, "Complexity analysis of fde receivers for massive mimo block transmission systems," *IET Communications*, vol. 13, Apr. 2019. DOI: 10.1049/iet-com.2018.5156.

[44] F. C. Vilar, "Implementation Of Zero Forcing And Mmse Equalization Techniques In OFDM," *Universidade de Fortaleza*, 2014.

[45] T. Levanen, K. Ranta-Aho, J. Kaikkonen, S. Nielsen, K. Pajukoski, M. Renfors, and M. Valkama, "5g new radio uplink performance: Noise, interference and emission constraints," in *2018 IEEE Wireless Communications and Networking Conference (WCNC)*, 2018, pp. 1–6. DOI: 10.1109/WCNC.2018.8377161.

[46] N. Benvenuto and S. Tomasin, "Iterative design and detection of a dfe in the frequency domain," *IEEE Transactions on Communications*, vol. 53, no. 11, pp. 1867–1875, 2005. DOI: 10.1109/TCOMM.2005.858666.

[47] P. Pedrosa, R. Dinis, F. Nunes, and A. Rodrigues, "Joint turbo frequency domain equalization and stochastic recursive filtering carrier synchronization," in *2015 IEEE 81st Vehicular Technology Conference (VTC Spring)*, 2015, pp. 1–5. DOI: 10.1109/VTCSpring.2015.7145907.

[48] F. Silva, R. Dinis, and P. Montezuma, "Estimation of the Feedback Reliability for IB-DFE Receivers," *ISRN Communications and Networking*, vol. 2011, pp. 1–7, Aug. 2011, ISSN: 2090-4355. DOI: 10.5402/2011/980830.

[49] R. Dinis, T. Araújo, P. Pedrosa, and F. Nunes, "Transmission systems: Joint turbo equalisation and carrier synchronisation for SC-FDE schemes," *European Transactions on Telecommunications*, vol. 21, no. 2, pp. 131–141, Mar. 2010, ISSN: 1124318X. DOI: 10.1002/ett.1377. [Online]. Available: https://repositorio.ual.pt/handle/11144/3729.

[50] A. Gusmao, P. Torres, R. Dinis, and N. Esteves, "A turbo fde technique for reduced-cp sc-based block transmission systems," *Communications, IEEE Transactions on*, vol. 55, pp. 16–20, Feb. 2007. DOI: 10.1109/TCOMM.2006.887482.

[51] G. J. Foschini and M. J. Gans, "On Limits of Wireless Communications in a Fading Environment when Using Multiple Antennas," *Wireless Personal Communications*, vol. 6, no. 3, pp. 311–335, 1998, ISSN: 09296212. DOI: 10.1023/A:1008889222784. [Online]. Available: https://doi.org/10.1023/A:1008889222784.

[52] F. Siddiqui, F. Danilo-Lemoine, and D. Falconer, "Iterative interference cancellation and channel estimation for mobile sc-fde systems," *IEEE Communications Letters*, vol. 12, no. 10, pp. 746–748, 2008. DOI: 10.1109/LCOMM.2008.080262.

[53] A. Silva, J. Assunção, R. Dinis, and A. Gameiro, "Performance evaluation of IB-DFE-based strategies for SC-FDMA systems," *Eurasip Journal on Wireless Communications and Networking*, vol. 2013, no. 1, pp. 1–10, 2013, ISSN: 16871472. DOI: 10.1186/1687-1499-2013-292.

Appendix - A

Table A.1: Sampling frequency and FFT length for normal CP, FR1, with SCS 15 kHz [28]

Channel BW $[MHz]$	Total Subcarriers (N^{μ}_{FFT})	Data Subcarries (N^{μ}_{d})	Sampling Freq. $[MHz]$ (F^{μ}_{s})
5	512	300	7.68
10	1024	624	15.36
15	1536	948	23.04
20	2048	1272	30.72
25	2048	1596	30.72
30	3072	1920	46.08
40	4096	2592	61.44
50	4096	3240	61.44

Table A.2: Sampling frequency and FFT length for normal CP, FR1, with SCS 30 kHz [28]

Channel BW $[MHz]$	Total Subcarriers (N^{μ}_{FFT})	Data Subcarries (N^{μ}_{d})	Sampling Freq. $[MHz]$ (F^{μ}_{s})
5	256	132	7.68
10	512	288	15.36
15	768	456	23.04
20	1024	612	30.72
25	1024	780	30.72
30	1536	936	46.08
40	2048	1272	61.44
50	2048	1596	61.44
60	3072	1944	92.16
70	3072	2268	92.16
80	4096	2604	122.88
90	4096	2940	122.88
100	4096	3276	122.88

Table A.3: Sampling frequency and FFT length for normal CP, FR1, with SCS 60 kHz [28]

Channel BW $[MHz]$	Total Subcarriers (N^{μ}_{FFT})	Data Subcarries (N^{μ}_{d})	Sampling Freq. $[MHz]$ (F^{μ}_{s})
10	256	132	15.36
15	512	216	30.72
20	512	288	30.72
25	768	372	40.08
30	768	456	40.08
40	1024	612	61.44
50	1024	780	61.44
60	1536	948	92.16
70	1536	1116	92.16
80	2048	1284	122.88
90	2048	1452	122.88
100	2048	1620	122.88

Table A.4: Sampling frequency and FFT length for normal CP,FR2,with SCS 60 and 120 kHz [28]

SCP $[KHz]$	Channel BW $[MHz]$	Total Subcarriers (N^{μ}_{FFT})	Data Subcarries (N^{μ}_{d})	Sampling Freq. $[MHz]$ (F^{μ}_{s})
60	50	256	132	15.36
	100	512	216	30.72
	200	512	288	30.72
120	50	768	372	40.08
	100	768	456	40.08
	200	1024	612	61.44
	400	1024	780	61.44